ISBN 978-82-326-5210-5 (printed ver.)
ISBN 978-82-326-6010-0 (electronic ver.)
ISSN 1503-8181 (printed ver.)
ISSN 2703-8084 (electronic ver.)

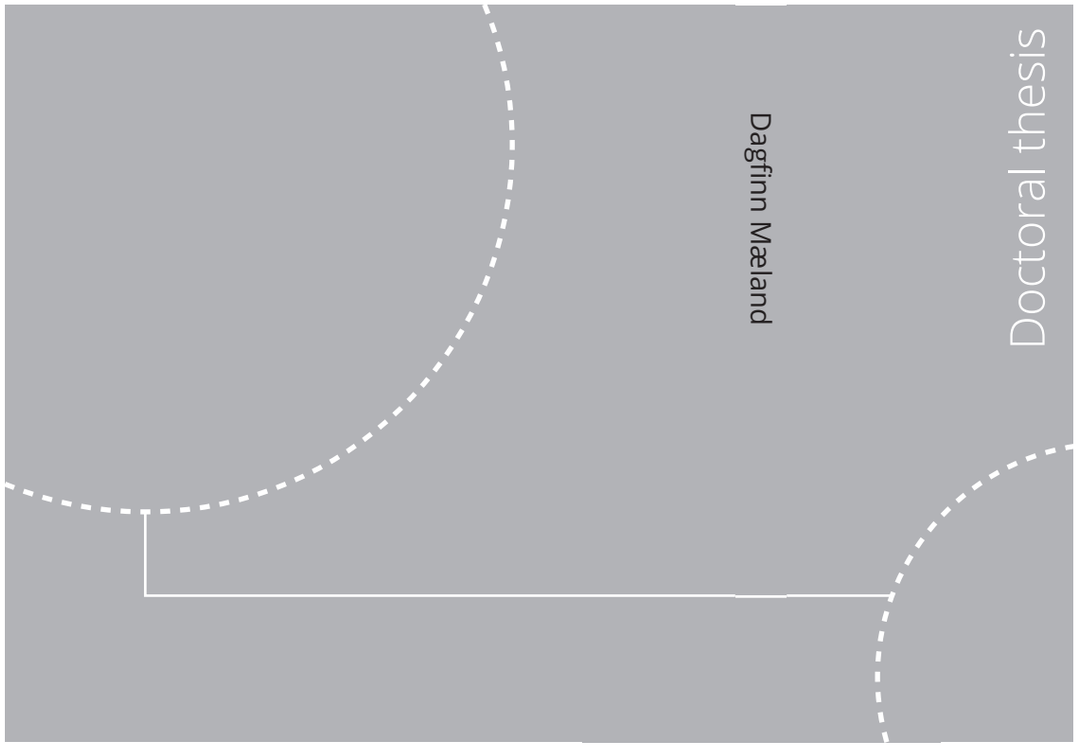

Doctoral theses at NTNU, 2022:46

Dagfinn Mæland

Wet gas centrifugal compressor performance evaluation

Doctoral theses at NTNU, 2022:46

NTNU

Norwegian University of Science and Technology

NTNU
Norwegian University of Science and Technology
Thesis for the degree of Philosophiae Doctor
Faculty of Engineering
Department of Energy and Process Engineering

NTNU

Norwegian University of Science and Technology

Dagfinn Mæland

Wet gas centrifugal compressor performance evaluation

Thesis for the degree of Philosophiae Doctor

Trondheim, February 2022

Norwegian University of Science and Technology
Faculty of Engineering
Department of Energy and Process Engineering

NTNU
Norwegian University of
Science and Technology

NTNU
Norwegian University of Science and Technology

Thesis for the degree of Philosophiae Doctor

Faculty of Engineering
Department of Energy and Process Engineering

ISBN 978-82-326-5210-5 (printed ver.)
ISBN 978-82-326-6010-0 (electronic ver.)
ISSN 1503-8181 (printed ver.)
ISSN 2703-8084 (electronic ver.)

Doctoral theses at NTNU, 2022:46

PRINTED IN NORWAY
NO - 1598

NORDIC SWAN ECOLABEL
Printed matter
2041 0731

Printed by Skipnes Kommunikasjon AS

ABSTRACT

The demand for oil and gas from the maturing Norwegian continental shelf (NCS) remains high. Even though the concern for climate change is shifting energy production towards renewables, production on the NCS is expected to continue for decades to come. If carbon capture and storage is managed and combined with technologies, such as conversion from hydrocarbon to hydrogen, production could be extended even further.

Wet gas compression, especially for subsea installations, is a promising technology for both new and existing fields. It can enable the tie-in of remote reservoirs to the existing infrastructure and allow for simplified process solutions thus possibly reducing both investment and operational costs. Furthermore, by locating compressor stations near the subsea well head increased recovery can be achieved because the well can be produced at a lower pressure compared to topside compression.

A prerequisite for the successful installation of subsea wet gas compression is exceptionally reliable solutions, due to the excessive cost of any intervention. It is thus necessary to increase knowledge on key aspects of the system, such as rotor dynamics, transient behaviour, performance and fouling.

The focus of this thesis has been to investigate how wet gas affects the performance of centrifugal compressors, how performance parameters should be established and to investigate if models can be built that allow for correction between different wet operating conditions. Experimental results were partly obtained from the test rig at the Norwegian University of Science and Technology (NTNU) and partly from Equinor's test facility at K-Lab. The NTNU open-loop test rig has a single impeller centrifugal compressor and runs on water and air under ambient conditions. Equinor's test facility at K-Lab has two full-scale test loops that operate at high pressures and temperatures and utilize mixtures of hydrocarbon gas, condensate and water.

As regards wet gas compressors, there is currently limited knowledge on how the performance will shift for changing inlet conditions. Therefore, the vendors are unable to estimate performance for a specific wet inlet condition a priori. Furthermore, no international standard has been established that specifies how to evaluate wet performance. Indeed, much work is required to sufficiently describe the performance and test procedure for wet gas performance. The current work aims to illuminate key areas of wet gas performance for the design, test, and operational phases.

When it comes to the design and testing of wet gas compressors, it is not clear how to compare results between different operating conditions, such as test and real operation. This problem was analysed first by reviewing the dry gas similarity theory and then expanding these concepts to include wet gas. Finally, the appropriateness of such expansion from dry to wet gas was discussed. This work documents that Type2 testing (large difference between test and specified condition) can be difficult to achieve for wet gas compressors.

A two-impeller wet gas centrifugal compressor was tested at K-Lab. The performance test results were analysed and key factors affecting performance parameters were identified. Furthermore, a model for wet gas performance based on these parameters was created. The method used to address this issue was a combination of regression and minimization of an objective function. The proposed model showed the capability of collecting the data points obtained under different operating conditions onto a "performance surface" with good precision.

Limited knowledge exists about how uncertainties propagate through a complex wet gas test loop, such as the VGII loop at K-Lab, and eventually result in uncertainties of wet gas performance parameters in general. To address this issue the Monte Carlo method was used in combination with a sensitivity analysis. In this way, the uncertainties could be propagated through the entire system. Thus, standard uncertainties and coverage intervals for the performance parameters could be established, as well as the identification of key input parameters that affect these uncertainties. Somewhat elevated uncertainties were found for the wet compared to dry conditions, but still within reasonable limits. Furthermore, many of the performance parameters are highly sensitive to inlet and discharge temperature, especially those relying on enthalpies. By including a torque meter and a gas density meter in the wet gas test facility, these uncertainties could be significantly reduced.

The detrimental effect of fouling on wet gas compressor performance was observed during testing at K-Lab. To further investigate this effect, a fouling test under controlled conditions was conducted at NTNU. The experimental results show that wet performance characteristics are heavily affected by flow path fouling. Furthermore, to quantify how the wet performance is affected by the fouling, a model was developed to correct all the efficiency curves to the dry clean curve. The model was able to collect the spread between clean and fouled curves for the same *GMF*.

ACKNOWLEDGEMENTS

First and foremost, I would like to thank my parents for all their love and support throughout my life. Thank you for always being available, for always supporting me and always believing in me throughout my studies.

I am grateful for the opportunity to conduct part-time PhD-studies at NTNU while maintaining my position as an engineer at Equinor's test facility at K-Lab. Over these years I have had the opportunity to develop my knowledge. Furthermore, I have had the opportunity to develop and run tests at the NTNU impeller test rig as well as taking part of the planning and execution of full-scale wet gas compressor tests at K-Lab.

I would like to thank my employer Equinor ASA for supporting the ongoing program relating to wet gas compressor fundamentals, for their support of the test rig modification, and for providing valuable industrial application challenges to the fundamental research. Also, thanks to my leaders in Equinor throughout my PhD period, Rainish Sharma, Kjetil Veslestøl Tveito, and Jarle Søvik for always supporting me when challenges have arisen.

A special thanks to my supervisor Professor Lars E. Bakken for his guidance, advice and for always being available when I needed support. Thanks for your cheerful outlook and good humour that is always heartening. I would also like to thank my co-supervisor Tor Bjørge for valuable support and discussions relating to thermodynamics, and Håvard Nordhus for supporting my work and for valuable input relating to PVT simulations.

I would also like to thank my good friend Øystein Ariansen Haaland for his conversations and advice on regression.

Thanks to Øyvind Hundseid, Martin Bakken and Levi André B Vigdal for valuable and interesting discussions relating to the field. Additionally, I would like to thank Erik Langørgen for his expertise on professional rig operation and modifications.

A special thanks also goes to Ranheim IL's supporter club personified by Even Solbraa and Peter Sassan Johansson for valuable conversations about PVT simulations and valuable input relating to pipe flow.

Thanks to all my fantastic colleagues at K-Lab, thanks for letting me be part of the wonderful work environment and for always being positive and supporting my work. Special thanks to Christian Hågenvik and Terje Staveland for valuable discussions relating to wet gas testing and PVT related issues.

The task of completing a PhD is a long and lonesome journey. I have tried to protect my family from the strain of my work, but I know that I have sometimes been absent both physically and mentally. I want to thank my children Njål, Ada, and Live for their patience. And finally, a loving thanks to my wife Christine for all the support, patience and understanding throughout these years. I love you.

LIST OF PAPERS

I. D. Mæland, L. E. Bakken, “Wet gas compression – Test conditions and similitude”, ASME Turbo Expo 2017, GT2017-64374.

II. D. Mæland, L. E. Bakken, “Wet gas compressor testing – Performance uncertainty”, IMECE2020, IMECE2020-23711.

III. D. Mæland, L. E. Bakken, “Fouling effects on wet gas compressor performance: An experimental investigation”, ASME Turbo Expo 2021, GT2021- 59543

IV. D. Mæland, L. E. Bakken, “Wet gas hydrocarbon centrifugal compressor – Performance test results and evaluation”, IMECE2021, IMECE2021-71344.

TABLE OF CONTENTS

LIST OF FIGURES

LIST OF TABLES

NOMENCLATURE

Symbol	*Description*	*Unit*
A	Area	[m^2]
a	Speed of sound	[m/s]
b	Impeller exit width	[m]
C	Fluid velocity	[m/s]
D	Diameter	[m]
Dr	Density ratio	[-]
f	Darcy friction factor	
GMF	Gas Mass Fraction	[-]
GVF	Gas Volume fraction	[-]
h	Specific enthalpy	[kJ/kg]
h_p	Polytropic head	[kJ/kg]
Δh	Specific enthalpy change	[kJ/kg]
Δh_F	Specific enthalpy loss due to friction	[kJ/kg]
k_s	Equivalent sand roughness	[m]
L	Length	[m]
LMF	Liquid mass fraction	[-]
M	Molar mass	[kg/kmol]
Ma	Mach number	[-]
m	Mass loaded into loop	[kg]
$\dot{m}$	Mass flow	[kg/s]
N	Rotational speed	[s^{-1}]
n	Polytropic exponent	[-]
P	Power	[kW]
PVF	Phase volume fraction	[-]
p	Pressure	[Pa]
p_r	Pressure ratio	[-]
Δp_F	Pressure loss caused by friction	[Pa]
Q	Volume flow	[m^3/s]
r	Radius	[m]
R_a	Mean surface roughness	[m]
Re	Reynolds number	[-]
s	Standard deviation of data	
s	Specific entropy	[kJ/(kg·K)]
T	Temperature	[K]
U	Impeller tip speed	[m/s]
V	Velocity of flow	[m/s]
X	Mole Fraction	[-]
y	Distance from the mean line	[m]

Greek Symbols

Symbol	*Description*	*Unit*
α	Void fraction	[-]
Γ	Wet regression variable	[-]
ζ	Non-friction losses	[-]
η_p	Polytropic efficiency	[-]
η	Efficiency	[-]
θ	Sensitivity	
μ	Polytropic head coefficient	[-]
μ	Dynamic viscosity	[Pa·s]
ν	Specific volume	[m^3/kg]
ρ	Density	[kg/m^3]
σ	True standard deviation of population	

σ	Surface tension	[N/m]
τ	Work coefficient	[-]
ϕ	Flow coefficient	[-]

Superscripts

Symbol	*Description*
σ	Sigma-normalized

Subscripts

Symbol	*Description*
*	Note
CR	Critical
D	Droplet
d	Compressor discharge
d	Droplet
F	Film
f_{indep}	Friction independent
g	Gas phase
l	Liquid phase (oil/water mixture)
M	Mechanically determined
m	Homogeneous gas-liquid mixture
o	Oil phase
sp	Specified condition
T	Themodynamically determined
t	Test condition
w	Water phase
wet	Wet gas property
1	Compressor inlet
2	Compressor discharge
eye	Impeller eye
tip	Impeller tip

Acronym

Symbol	*Description*
AMB	Active Magnetic Bearing
API	Application programming interface
CAPEX	Capital expenditure
CPA	Cubic-Plus-Association
HV	Huron-Vidal
ICAAMC	International Compressed Air and Allied Machinery Committee
MCM	Monte Carlo method
NTNU	Norwegian University of Science and Technology
NCS	Norwegian continental shelf
OPEX	Operational expenditure
PDF	Probability density function
PR78	Peng–Robinson 78
PVT	Pressure Volume Temperature
SA	Sensitivity analysis
SRK	Soave−Redlich−Kwong
SST	Subsea Test
VSD	Variable Speed Drive
VGII	Wet gas 2 (translated)

1 INTRODUCTION

This thesis focuses on how liquid affects centrifugal wet gas compressor performance. The work is based on theoretical considerations, thermodynamic simulations and experimental test results. Experimental results were obtained both from the test rig at the Norwegian University of Science and Technology (NTNU) and from Equinor's test facility at K-Lab. The NTNU open-loop test rig has a single impeller centrifugal compressor and is operating on water and air under ambient conditions. Equinor's test facility at K-Lab has two full-scale test loops that operate at high pressures and temperatures, and use mixtures of hydrocarbon gas, condensate and water. In this chapter, the work will be put into a broader context and the scope of work, as well as the limitations of the work, are outlined.

1.1 Background

The demand for oil and gas remains high and production from the Norwegian continental shelf (NCS) is expected to increase in the coming years. This is illustrated by Figure 1, where historical data are provided together with a production forecast from the Norwegian Petroleum Directorate [1].

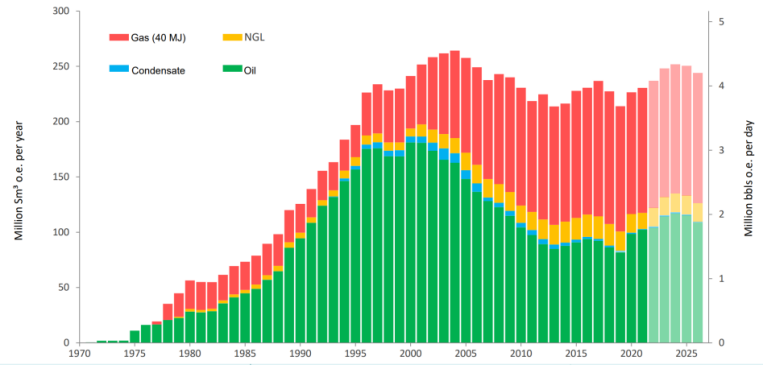

Figure 1: History and forecast of oil and gas production on NCS [1]

As the NCS and other areas of exploration and production mature, production is shifting from being oil dominant to being gas dominant and a large portion of wells are producing what can be characterized as wet gas fluid. Wet gas is often defined as a mixture of gas and liquid with a liquid fraction below 5% by volume. Production from wet gas wells is typically routed to existing infrastructure, such as pipelines, offshore, or onshore processing plants. Several factors determine whether wet gas wells can produce into existing infrastructure and how much can be extracted from them. Firstly, the significant pressure loss associated with wet gas pipe flow limits the possible transportation length for a given well pressure. Secondly, as production from a wet gas well declines, the gas velocity becomes too low to maintain a stable flow regime and unfavourable scenarios like slug flow may occur posing considerable strain on the infrastructure. Installation of a wet gas compressor station in proximity to the well can mitigate the above-mentioned problems.

Typically, a two-phase flow is separated upstream compression. Separation systems have a large footprint and entail substantial weight and cost. Wet gas compression technology is attractive to the oil and gas producers as it attempts to reduce the complexity by removing equipment such as scrubbers and pumps. Thus, wet gas compression can potentially reduce both capital expenditure (CAPEX) and operational expenditure (OPEX). Furthermore, the installation of a compressor near the well gives increased recovery because the well pressure can be reduced. However, challenges relating to wet gas compression need to be addressed before the technology becomes commercially accepted as a viable solution. Some of the challenges are listed below:

Materials: Stress resistant materials that can handle the increased loads due to liquids are necessary. Erosion resistance is needed on all surfaces where wet gas will impact the materials at a high velocity and corrosion resistance is required on all wetted parts throughout the machine. Stress corrosion cracking and pitting corrosion need special attention. In the case of integrated motor compressors, to avoid corrosion and short circuits, the motor casing and insulation materials also need to handle trace amounts of liquid passing the cooling gas system and entering the motor casing.

Mechanical Design: Rotor bearings need to be designed to handle any influence the liquid might have on the rotor dynamics. Labyrinths need to handle wet gas and still be able to maintain acceptable damping and stiffness. Furthermore, labyrinths must be designed to avoid fouling. In the case of integrated motor-compressors, the mechanical design of the motor must be sufficiently robust to handle additional vibrations originating from the compressor.

Performance: Aspects relating to the evaluation of wet gas compressor performance are the focus of this thesis. There are several challenges concerning this topic. These are linked to design, testing, and operation. ***Design phase:*** At present, compressor vendors do not have the knowledge to design a compressor that will meet a specified wet gas performance, though some manufacturers are in the process of developing such tools. Efforts must be focused on these issues if future wet gas compressors are to be designed with predictable wet gas performance of sufficient accuracy. ***Test Phase:*** No acknowledged standard currently exists for how to conduct performance testing on a wet gas compressor. It is also uncertain whether an ASME PTC10 [2] Type 2 performance test can be used to determine the actual performance of a wet gas compressor, or whether a Type 1 performance test is the only viable option. ***Operating phase****:* A prerequisite for successful implementation of subsea wet gas compressors is high reliability, thus knowledge of possible failure modes is important. Compressor operating experiences show several challenges related to deterioration: some to internal wear, i.e., labyrinth clogging, material pitting and deformation, others to internal flow channel fouling. Furthermore, wet gas compressor operators will unavoidably meet changing inlet conditions. Thus, knowledge of how the shift in wet inlet conditions will affect performance will be of great interest for operational organizations as it will allow for estimation of power consumption, production capacity, etc.

As regards conventional dry gas compressor design, performance prediction is usually undertaken by the compressor manufacturer, using in-house know-how in impeller design and selection. This specialised knowledge is potentially unsuitable for predicting wet gas performance in the design phase; hence, a wet gas compressor may not meet the design requirements specified by the customer. A typical procedure for a dry gas compressor purchase is as follows: A compressor manufacturer is provided with compressor inlet conditions, such as actual inlet flow, pressure, temperature, and gas composition (other requirements such as design pressure, design temperature, etc., are also provided). Furthermore, the manufacturer is provided with the requirements for outlet pressure. The manufacturer then starts the design by selecting impeller(s) that match the requirements given by the customer. Following the manufacture of a dry gas machine, a standardized test, typically ASME PTC10 [2] or ISO 5389 [3], is performed to verify that the machine's performance meets contractual requirements. The standards allow for two types of tests: Type 1 test (same operating conditions at the specified and test point), and Type 2 test (different operating conditions at the specified and test point, where speed is selected to target for similarity conditions). To ensure similarity, permissible deviations between specified and test conditions in several parameters are required. These are specific volume ratio, flow coefficient, Machine Mach number and Machine Reynolds number. Type 2 tests are the most common performance test for dry compressors and are usually conducted at the manufacturer's premises. Results obtained from Type 2 tests are back-calculated to specified (guarantee) conditions, assuming similarity. Currently, compressor manufacturers do not have the knowledge to design a wet gas compressor that will reach a specific wet gas discharge condition, given the inlet conditions. Furthermore, no internationally established standards exist for the evaluation of wet gas compressor performance.

For a manufacturer to be able to predict the wet gas performance of a compressor a priori, and for operators to predict performance for varying operating conditions, detailed knowledge of how wet gas affects the performance is needed. Therefore, extensive testing is essential to collect data that will supply the fundamental knowledge to allow for better predictions in the future. A complicating factor for the prediction and evaluation of the wet gas performance of a hydrocarbon compressor is that the composition of the gas and the liquid is constantly changing throughout the machine due to phase transition. To illustrate the point, imagine a wet gas compressor running on a fixed inlet total composition. The inlet gas and oil composition and the gas mass fraction will be determined by the inlet pressure and temperature. The discharge gas and oil composition, as well as the gas mass fraction, will be determined by the inlet condition and the operating point. This contrasts with dry gas compression where the gas composition is constant throughout the compression process.

Fouling has a detrimental effect on compressor performance and can eventually cause mechanical damage to the machine. For wet gas compressors, especially for subsea operations, it is important to prevent fouling, as the maintenance cost is extremely high. Precipitation of solutes that can cause fouling needs to be avoided throughout the compressor and in downstream piping. If it cannot be avoided, a washing system should be installed as a mitigating measure. However, washing is not always possible as some depositions are not soluble in neither oil, water nor other solvents. In such situations, it is crucial to avoid operating conditions where precipitation of solutes can occur.

1.2 Subsea compression

As areas of exploration and production mature, production from existing fields is declining and there are fewer major discoveries. To maintain production and profitability, boosting to increase tail production as well as the tie-in of satellite fields is of crucial importance, as it allows for utilisation of existing production and transportation capacity. Installation of subsea wet gas compressors in such fields is promising for oil and gas producers as the technology can provide several advantages:

- As producing fields mature and pressure declines, typically the topside facilities are modified to allow for low pressure (LP) production. These include modification of compressor stations, separator equipment and piping. Installation of subsea compression may eliminate the need for topside modifications
- Installation of subsea compression for remote satellite fields will increase the allowable distance between the field and the existing production infrastructure.
- Increased recovery is achieved by installing compressors close to wells because production can be maintained at a lower well pressure.
- Pressure loss is reduced in transportation piping. This reduction is caused by increased density, which gives reduced velocities for the same mass flow, thus reducing pressure loss.
- Enabling production from dead wells has been demonstrated as a benefit of subsea compression [4]
- Health and safety risks associated with production can be reduced, as subsea equipment does not require manning offshore.
- Surge/slug flow can be avoided or postponed, as fluid velocity can be increased by the compressor, which in practice reduces the liquid content in the flowline. This applies both to upstream and downstream compressors.

The following is a brief introduction to subsea concepts either currently in operation or approved for development.

1.2.1 Åsgard subsea compression

The Åsgard subsea station consists of two compressor trains producing from Mikkel and Midgard wells to the Åsgard B platform. It was the world's first subsea compressor system in operation when it came onstream in 2015. Two MAN HOFIM machines were installed, each with a power of 11.5 MW. As illustrated in Figure 2, these are integrated motor-compressors without gearboxes. The machines are hermetically sealed, oil-free, with magnetic bearings. The machines are qualified at K-Lab for wet gas operation and have been extensively tested with LMF up to 30%. Figure 3 shows the pilot module as it was lifted into the test pit at K-Lab. The Åsgard subsea trains have liquid scrubbers and pump modules and are not continuously operated in wet gas, but regularly use washing sequences to prevent fouling. A detailed outline of the technology qualification program has been provided by Kleynhans et al.[5] and information on the operational experience has been documented by Hedne et al. [6].

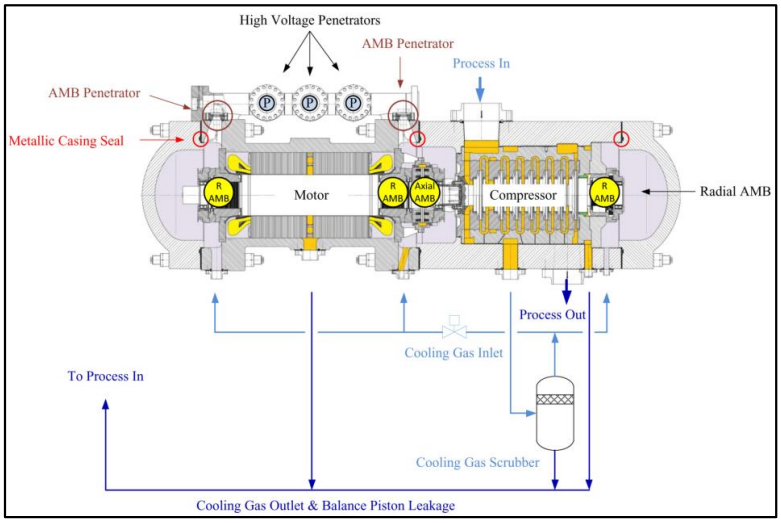

Figure 2 MAN oil-free, hermetically sealed HOFIM [5]

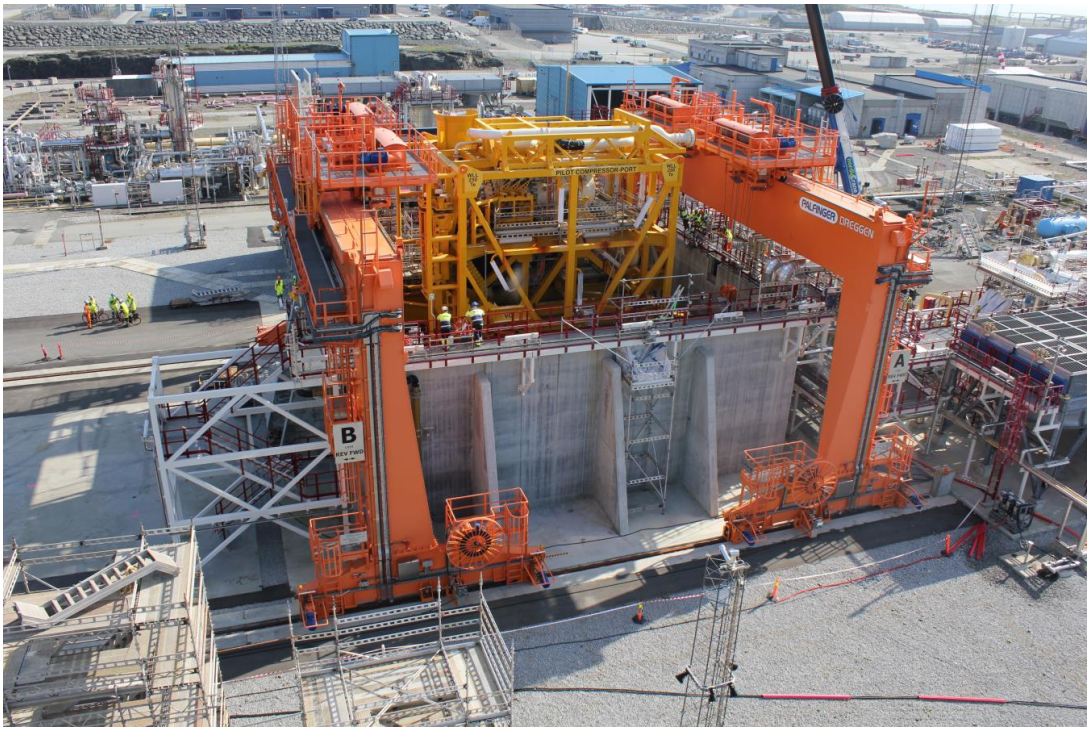

Figure 3 Åsgard subsea compressor pilot module lifted into test pit at K-Lab

1.2.2 Gullfaks subsea compression

The Gullfaks subsea compression station has two compressors in parallel operation. The process design allows for series operation intended for lower flow rates (in tail production) when a higher head is required. The installed machines are of the type OneSubsea WGC4000 contra-rotating axial compressors, which are designed for wet gas. The compressors were installed in 2015 and have been in operation since 2017. The system is operating on the well stream without liquid separation upstream of the compressor. Each machine is driven by 2x2.5MW motors that are filled with a hydraulic barrier fluid. WGC4000 can handle *GMF* between 0 to 100%.

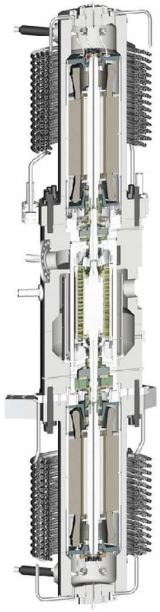

Figure 4 OneSubsea WGC4000 [4]

Detailed information on the technology qualification program has been outlined by Hjelmeland and Torkildsen [7], whereas operational experience has been documented by Bøe et al. [4].

1.2.3 Ormen Lange wet gas subsea compression project

The license partners of the Ormen Lange have given a final investment decision on a wet gas subsea compression project at Ormen Lange. The compressor stations will be installed at a water depth of 900 meters, 120 km from shore. The compressors will be powered from shore, thus giving a 120 km power step-out. The compressors to be installed are OneSubsea contra-rotating axial compressors.

The project is estimated to give an added production between 30-50 billion standard cubic meters (bcm) of natural gas, increasing Ormen Lange's overall gas recovery factor from 75 to 85 percent.

1.2.4 Jansz-Io gas subsea compression project

At the Chevron-operated Jansz-Io gas field, 200 km offshore Western Australia, it has been decided to develop a subsea compression station at a water depth of 1350 m. The EPC contractor, Aker Solutions, has awarded MAN Energy Solution the contract to supply 5 HOFIM machines for the project (3 for operation and 2 spare). [8]

1.3 Scope of work

The field of wet gas compression is relatively new, and a solid theoretical foundation is lacking. The knowledge gap is especially true for wet gas performance evaluation. Thus, several aspects relating to the design phase, performance testing and the operating phase call for further investigation.

The main objectives are

- Analyse how wet gas performance can be compared between different inlet conditions. When designing and testing a wet gas compressor, how to validate that the tested performance will reflect the actual operating performance.
- Analyse test results obtained from a two-impeller centrifugal compressor tested under realistic hydrocarbon conditions at K-Lab. Identify key wet parameters affecting performance and develop a model for wet performance based on these parameters.
- Investigate how the uncertainties of wet gas compressor performance parameters are propagating through a full-scale wet gas test loop, operating under realistic conditions. Additionally, the aim was to identify key input parameters that affect the uncertainty of performance parameters via a sensitivity analysis.
- Experimentally investigate how fouling affects wet gas compressor performance. The purpose was to document the fouling effects and to develop a first approach model for fouling correction.

1.4 Limitations

Centrifugal compressors cover an extensive range of design parameters, such as suction pressures, flow rates, temperatures, heads, and fluid compositions. Large variations in operational range will also be the case for wet gas compressors in the future. The physical constraints of the test facilities will thus naturally impose limitations on the experimental tests and analysis. The limitations of this work are summarized below.

- The PhD work is limited to performance evaluation of wet gas centrifugal compressors and the operational envelopes of the test facilities. The work is also limited to the performance characteristics of the single impeller compressor at the NTNU test loop and the two-impeller compressor at the K-Lab test loop.
- Wet gas performance analysis of experimental data has been limited to bulk properties, such as flow rates of gas and liquid, flange to flange measurements of pressures and temperatures, and shaft power measurements. Furthermore, densities and thermodynamic data have been simulated at flange conditions using appropriate PVT simulation software. However, to establish the properties at flange conditions, it is necessary to simulate substantial portions of the test loops.
- Compressor internal geometry is frozen upfront project start-up and hence not the object of revision.

1.5 Thesis outline

Chapter 1 - INTRODUCTION: Introduces the subject and puts it into context, presents the problem statement/scope of work and the limitation of the work

Chapter 2 - THEORETICAL FOUNDATIONS: Introduces the general wet gas theory applicable to the current work, followed by the wet gas performance analysis.

Chapter 3 - TEST FACILITIES: Presents the test facilities used for acquiring the experimental results.

Chapter 4 - METHOD DESCRIPTION FOR WET GAS COMPRESSOR ANALYSIS: Summarizes the methods used in this thesis

Chapter 5 - RESULTS AND DISCUSSION: Summarizes the results of the work.

Chapter 6 - CONCLUSION: Concludes the work

Chapter 7 - FURTHER WORK: Recommends further work

Paper I: D. Mæland, L. E. Bakken, “Wet gas compression – Test conditions and similitude”, ASME Turbo Expo 2017, GT2017-64374.

Paper II: D. Mæland, L. E. Bakken, “Wet gas compressor testing – Performance uncertainty”, IMECE2020, IMECE2020-23711.

Paper III: D. Mæland, L. E. Bakken, “Fouling effects on wet gas compressor performance: An experimental investigation”, ASME Turbo Expo 2021, GT2021- 59543

Paper IV: D. Mæland, L. E. Bakken, “Wet gas hydrocarbon centrifugal compressor – Performance test results and evaluation”, IMECE2021, IMECE2021-71344.

Appendix – A: Provides a brief introduction to cubic equations of state, mixing rules and flash calculations.

2 THEORETICAL FOUNDATIONS

This chapter introduces the theoretical foundations for the analysis of wet gas compressor performance. This includes an introduction to important wet gas parameters and the performance analysis itself.

2.1 Wet gas fundamentals

Wet gas flow is given as the low liquid content region of multiphase flow. In the context of compression, wet gas flow is often defined as the region between pure gas and 5% liquid by volume [9, 10]. However, other definitions relating to the Lockhart-Martinelli parameter are frequently used in the multiphase flow meter community [11], where the Lockhart-Martinelli parameter $X<0.3$ defines the limit for what is defined as wet gas flow. In the following sections, important parameters for the analysis of wet gas flow are outlined. The main analysis focuses on the homogeneous model, but several dimensionless parameters relating to phase slip and segregation are also introduced. Furthermore, thermodynamic equilibrium is assumed throughout this work when applying thermodynamic properties.

The homogeneous model treats the wet gas flow as a homogeneous mixture, i.e., all phases have equal velocities and thus the fluid is regarded as a single fluid and homogeneous mixed properties can be established.

The void fraction for a phase in a multiphase flow is defined as the cross-sectional area occupied by the phase to the total area

$$\alpha_k = \frac{A_k}{A} \tag{1}$$

Where A_k is the area occupied by the k-th phase and A is the total area available for the flowing fluid.

The phase volume fraction is defined as

$$PVF_k = \frac{Q_k}{\sum_k Q_k} \tag{2}$$

Where PVF is the phase volume fraction and Q_k is the volume flow rate of the k-th phase. The void fraction and the phase volume fraction become equal when all phases flow with the same velocity, which is true for the homogeneous flow model.

Similarly, the phase mass fraction can be defined as

$$PMF_k = \frac{\dot{m}_k}{\sum_k \dot{m}_k} \tag{3}$$

Where PMF is the phase mass fraction and $\dot{m}_k$ is the mass flow rate of the k-th phase.

Gas volume fraction (GVF) and gas mass fraction (GMF) are important parameters for the description of multiphase flow, and are special cases of Eq.(2) and Eq.(3), respectively. Assuming a flow consisting of gas, oil, and water phase they are given by

$$GVF = \frac{Q_g}{Q_g + Q_o + Q_w} \tag{4}$$

and

$$GMF = \frac{\dot{m}_g}{\dot{m}_g + \dot{m}_o + \dot{m}_w} \tag{5}$$

Here Q is volumetric flow rate, $\dot{m}$ is the mass flow and subscripts g, o, and w denotes the gas, oil and water phases, respectively. An interesting fact is that combining *GVF* and *GMF* provides an expression for the ratio of mixture density to gas density.

$$\frac{GVF}{GMF} = \frac{\sum_k \dot{m}_k}{\dot{m}_g}\frac{Q_g}{\sum_k Q_k} = \frac{1}{\rho_g}\frac{\sum_k \dot{m}_k}{\sum_k Q_k} = \frac{\rho_m}{\rho_g} \tag{6}$$

Where the last equal sign is true only under the homogeneous assumption.

The homogeneous density is given by the relation

$$\rho_m = \sum_k \alpha_k \rho_k \tag{7}$$

Where ρ are the densities and α are the void fractions. The subscripts m, and k denote the homogeneous mixture and phase number, respectively.

Liquid volume fraction (*LVF*) and liquid mass fraction (*LMF*) are often used in describing multiphase flow, here liquid is the combined liquid (typically oil and water phase) mass and volume flow fractions and given by

$$LVF = \frac{Q_o + Q_w}{Q_g + Q_o + Q_w} = 1 - GVF \tag{8}$$

and

$$LMF = \frac{\dot{m}_o + \dot{m}_w}{\dot{m}_g + \dot{m}_o + \dot{m}_w} = 1 - GMF \tag{9}$$

The density ratio between liquid and gas has also been identified as an important parameter influencing wet gas performance and is given by

$$Dr = \frac{\rho_l}{\rho_g} \tag{10}$$

For wet operating conditions where the liquid phase is a mixture of water and oil, the liquid density was calculated by the equation

$$\rho_l = \frac{Q_o\rho_o + Q_w\rho_w}{Q_o + Q_w} \tag{11}$$

Thus, the mixed liquid density property is calculated based on volumetric averaging.

The mixture enthalpy of a multiphase flow can be calculated by the mass-weighted enthalpy of the pure phases.

$$h_m = \sum_k PMF_k h_k \tag{12}$$

Here h_k is the enthalpy of the k-th phase. Typically, this is an available output from PVT software.

When the fluid viscosity increases, so do the internal losses of the compressor. Thus, it is important to have an estimate of the fluid viscosity in multiphase flow. For multiphase flow containing the three phases gas, oil, and water, the mixture viscosity was calculated by the equation

$$\mu_m = \frac{Q_g\mu_g + Q_o\mu_o + Q_w\mu_w}{Q_g + Q_o + Q_w} \tag{13}$$

Furthermore, under wet operating conditions where the liquid phase is a mixture of water and oil, the liquid mixture viscosity was calculated by the equation

$$\mu_l = \frac{Q_o\mu_o + Q_w\mu_w}{Q_o + Q_w} \tag{14}$$

Here the mixed viscosity property is calculated based on volumetric averaging. This expression is equal to the Duckler mixed viscosity for homogeneous gas-liquid flow [12].

Lockhart and Martinelli [13] developed a method for correlating the pressure drop in a two-phase flow to a dimensionless number. The original form of the Lockhart-Martinelli parameter X, for turbulent-turbulent flow is given by the equation

$$X^2 = \left(\frac{\dot{m}_l}{\dot{m}_g}\right)^{1.8}\left(\frac{\rho_g}{\rho_l}\right)\left(\frac{\mu_l}{\mu_g}\right)^{0.2} \tag{15}$$

It is important to note that different expressions for the Lockhart - Martinelli parameter are appropriate for different flow regimes and that new variants have been introduced over the years [11]. Thus, ambiguities easily arise when referring to the Lockhart - Martinelli parameter.

The presence of liquid will affect the speed of sound in the wet gas flow. As the Mach number is an important similarity parameter for compressor performance evaluation, an expression for the speed of sound in wet gas is also believed to play a significant role in wet gas compression [9, 14]. Woods model [15] for homogeneous speed of sound in wet gas is given by the equation

$$a_m = a_g \sqrt{\frac{1 + \frac{1-\alpha_g}{\alpha_g}}{\alpha_g \left(1 + \frac{1-\alpha_g}{\alpha_g}\frac{\rho_l}{\rho_g}\right)}} \tag{16}$$

Where a_g is the speed of sound of the gas phase.

By assuming that the Woods model represents the true speed of sound for the mixture, the machine Mach number for the homogeneous model can be given by

$$Ma_m = \frac{U_1}{a_m} \tag{17}$$

Where U_1 is the first impeller tip speed. This model for the homogeneous Mach number approaches the dry Mach number as the gas void fraction approaches unity. The Mach number, as defined by Wood's speed of sound, represents the homogeneous fluid compressibility effects. The shift in Mach number is included in the performance analysis, as it directly affects the stage pressure ratio and thereby the compressibility impact on fluid velocity triangles.

The Machine Reynolds number is a dimensionless number that represents the ratio of the inertia force to the viscous force. This number is an important similarity parameter and is associated with losses through the machine. The homogeneous machine Reynolds number can be described by the equation

$$Re_m = \frac{\rho_m U_1 b}{\mu_m} \tag{18}$$

This is similar to the Reynolds number for dry gas, but where the density and viscosity have been replaced with the expressions for homogeneous model mix phase quantities.

The Stokes number is a measure of the ability of droplets to follow the flow field and thus, can be regarded as a key factor for the description of wet gas flow. It is defined as the ratio of the response time of the droplets to the response time of the flow field, and for wet gas pipe flow it is given by the equation

$$St = \frac{\tau_d}{\tau_g} = \frac{\rho_d D_d^2 U_g}{18 \mu_g D} \tag{19}$$

Here, ρ_d and D_d is the density and diameter of the droplet. U_g and $\mu_g$is the velocity and dynamic viscosity of the gas phase and D is the pipe diameter. The Stokes number is dependent on the gas to liquid density ratio because the dynamic viscosity of the gas phase increases with increasing pressure. Within the impeller stage, impeller and diffuser section, the wet two-phase flow is exposed to high acceleration, deceleration and deflection that affect the flow field segregation and entrainment. In principle, the two-phase flow tends towards no slip as the Stokes number approaches zero.

The Weber number is a dimensionless number representing the ratio of inertia force to the surface tension forces. It is related to the comparison of dynamic pressure and internal droplet pressure caused by the surface tension. It is a measure of the breakup and formation of droplets and liquid film. For pipe flow, the Weber number can be expressed as

$$We = \frac{\rho_d U_g^2 D}{\sigma} \tag{20}$$

Here, σ is the surface tension between the droplet and the gas phase. The diameter D can either be the droplet diameter, or the diameter of the pipe depending on application[16].

There are several reasons why neither the Stokes number nor the Weber number can be used directly in the characterization of wet compressor performance. These are related to unknown values, such as the droplet diameter and the flow velocity. Also, to make use of such numbers for the description of wet gas compressor flow, an estimate of the droplet diameter is required. This is challenging as the droplet size will vary between inlet and outlet, as well as throughout the whole flow path of the machine. Furthermore, inside the machine, the flow will vary from mostly segregated to a more dispersed type of flow. Furthermore, the characteristic pipe diameters need to be replaced with a suitable value relating to the compressor design. One proposed solution is to replace the gas velocity with the impeller tip speed and the pipe diameter with the first impeller tip width. However, a method for estimating a representative droplet diameter will also be needed at least for the Stokes number.

2.2 Wet gas performance analysis

In the following section, the polytropic analysis is put into a historical context and its validity and suitability for wet gas compression are discussed.

When evaluating the performance of a compressor, a suitable reversible reference process is useful for investigating the efficiency of the machine. One natural choice of such a reference process could be the isentropic process. However, as outlined by Shultz [17], the thermodynamic relation

$$\left(\frac{\partial h}{\partial s}\right)_P = T \tag{21}$$

is associated with diverging pressure lines in the enthalpy-entropy diagram. This effect is depicted in the hs-diagram of a hydrocarbon gas mixture in Figure 5. These diverging lines lead to the effect that the stage efficiency for a multistage compressor does not match the overall efficiency. Thus, a compressor operating at similar inlet conditions but on different pressure lines would yield different isentropic efficiency.

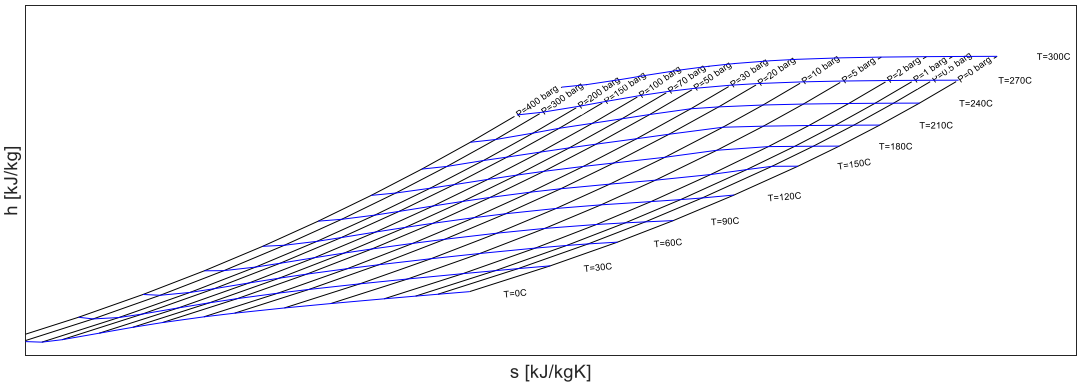

Figure 5 HS diagram for Hydrocarbon gas mixture

This problem, at least for dry gas compressors, is mitigated by the polytropic analysis. Thus, the polytropic process is the reference process of choice. To the authors' knowledge, the polytropic process was first introduced by Gustav Zeuner [18]. He derived the expression:

$$pv^n = constant \tag{22}$$

which he coined the polytropic curve. He also states that the exponent, n, is a constant. From this expression, the polytropic exponent for a process between states 1 and 2 is given by the expression

$$n = \frac{\ln\left(\frac{p_2}{p_1}\right)}{\ln\left(\frac{v_1}{v_2}\right)} \tag{23}$$

Here $v = 1/\rho$ is the fluid specific volume, p is pressure and subscripts denote state 1 and state 2, respectively. The polytropic work between these states is found by the integration of the work function along the polytropic path

$$h_p = \int_1^2 v dp \ , \qquad \text{where } pv^n = constant \tag{24}$$

Integration under this constraint gives the following expression for the polytropic head

$$h_p = \frac{n}{n-1}(p_2 v_2 - p_1 v_1) \tag{25}$$

This expression is exact for the definition of the polytropic process given by Eq.(22). Furthermore, the polytropic efficiency is defined as the ratio of the polytropic head to the enthalpy change between state 1 and state 2.

$$\eta_p = \frac{h_p}{h_2 - h_1} \tag{26}$$

However, in his polytropic analysis, Schultz [17] instead defines the path equation by constant efficiency

$$\eta_p = v\frac{dp}{dh} \tag{27}$$

where h is the specific enthalpy. Thus, the polytropic exponent n is no longer a constant and he developed a method for evaluating the variability of n. As numerical methods became available, Huntington [19] suggested a method for direct integration of $h_p = \int_1^2 v dp$ under the constraint of constant efficiency as a favourable method for the polytropic analysis. Figure 6 illustrates the direct integration path in the enthalpy-entropy diagram.

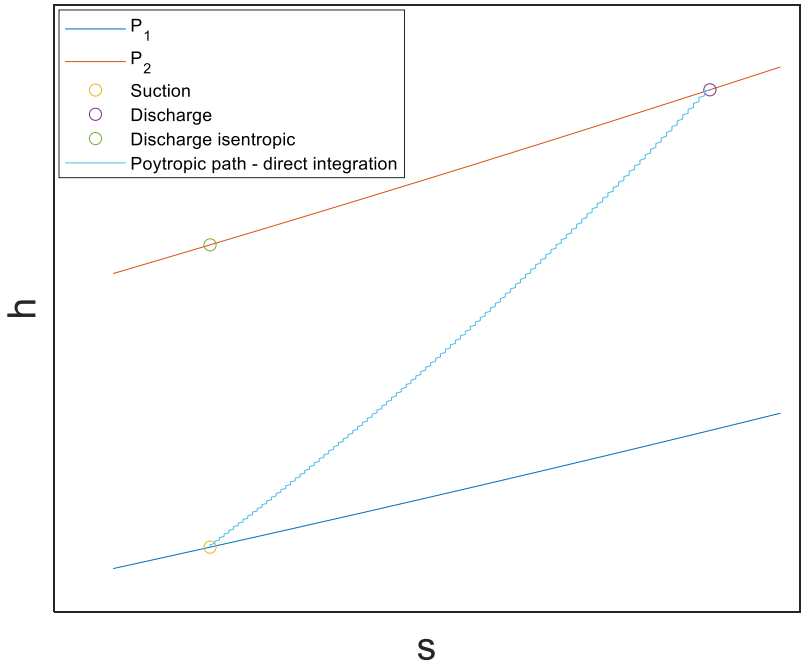

Figure 6 Direct integration

Figure 7 illustrates the different compression paths. Here the isentropic path is given together with the two polytropic paths defined by direct integration (constant efficiency constraint), and $pv^n = constant$ constraint, respectively.

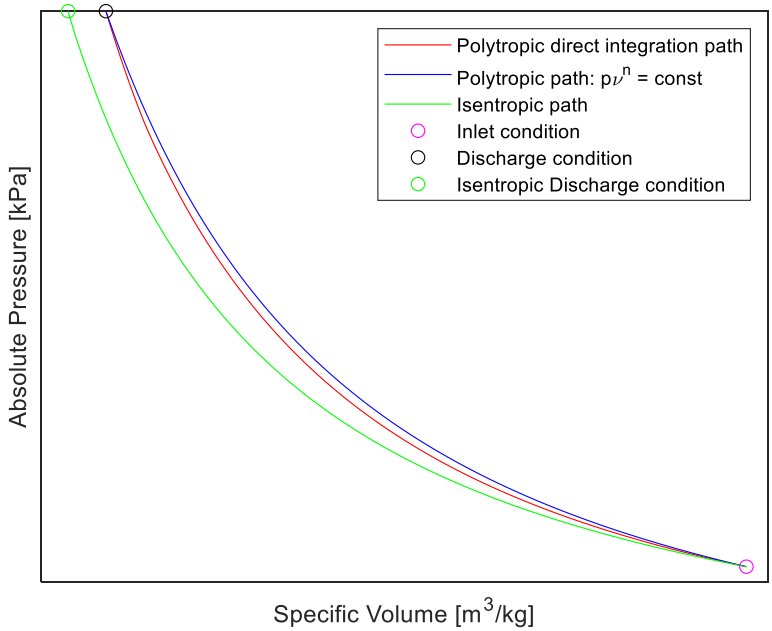

Figure 7 Different compression paths

Differing definitions of the polytropic process have given rise to ambiguities and misunderstandings and it has been argued that defining the polytropic path as the constant efficiency path is based on a faulty premise and that it is not a polytrope [20].

Some authors have suggested a two-fluid model for the wet gas polytropic head [21, 22]. Here, the liquid phase and the gas phase are treated separately and the expression for the polytropic head for the two-fluid model is given by:

$$h_p = LMF\left(\frac{p_2 - p_1}{\rho_l}\right) + (1 - LMF)\frac{n}{n-1}(p_2 v_2 - p_1 v_1) \tag{28}$$

There are some clear issues relating to the use of this expression. Due to phase transition, the liquid composition is not the same at the inlet and discharge and the same is true for the gas composition. Therefore, an error is introduced when using this expression because the composition that is needed to calculate the densities is not uniquely defined. It is important to remember that phase transition is especially large for high-pressure ratio machines, thus the problem will increase for such machines.

Based on the above discussion, we chose to use the original definition of the polytropic curve as given by Eq.(22) and use Eq.(23), Eq.(25), and Eq.(26) for the evaluation of polytropic performance. According to Wilsak and Tatara [20], these equations are valid under the assumptions of steady-state, single-phase and no chemical reaction. However, in our analysis, we will consider the homogeneous model, and because the path equation given by Eq.(22) is unambiguously defined also for the homogeneous model, we assume validity. In practice, this is done by replacing the densities at inlet and discharge in Eq.(23) and Eq.(25) with the homogeneous mixed density and the specific enthalpies in equation Eq.(26) with the homogeneous mixture enthalpies.

Several other dimensionless parameters other than the polytropic efficiency need to be defined for our analysis. The polytropic head coefficient is given by the expression

$$\mu_p = \frac{h_p}{\Sigma_i U_i^2} \tag{29}$$

where U_i is the tip speed of the i-th impeller. The flow coefficient is defined by the expression

$$\phi = \frac{4Q_1}{\pi D_1^2 U_1} \tag{30}$$

Where Q_1 is the volumetric flow rate at the compressor inlet, D_1 is the first impeller diameter, and U_1 is the tip speed of the first impeller.

The wet flow coefficient is thus defined as

$$\phi_{wet} = \frac{4(Q_g + Q_w + Q_o)}{\pi D_1^2 U_1} \tag{31}$$

Where Q_g is the inlet volumetric flow rate of the gas phase, Q_w is the inlet volumetric flow rate of the water phase, and Q_o is the inlet volumetric flow rate of the oil phase.

3 TEST FACILITIES

The topic of wet gas compression is a relatively new area of investigation. Theoretical foundations have not been fully established and therefore, there is a great need for test facilities. These facilities can produce the data needed to verify existing theories and more data will also form the basis for the development of new theories. Thus, the data produced from test facilities will drive the level of knowledge in the field upwards. The experimental results presented in this thesis have been gathered from test campaigns run at either the NTNU test rig or at the K-Lab test facility. In this chapter, a brief introduction to the test facilities is given together with an overview of the advantages and challenges relating to each type of facility.

3.1 NTNU Test Facility

The compressor test rig at NTNU is an open-loop facility, consisting of a centrifugal compressor with visualisation slots to the impeller inlet, diffuser, and volute section. The instrumentation is installed according to ASME PTC10 for performance testing. The compressor is driven by a 450 kW variable-speed electric motor. The experimental fluid is a low-pressure mixture of ambient air and water. A process flow diagram of the test rig is given in Figure 8, and Table 1 shows the rig operating conditions.

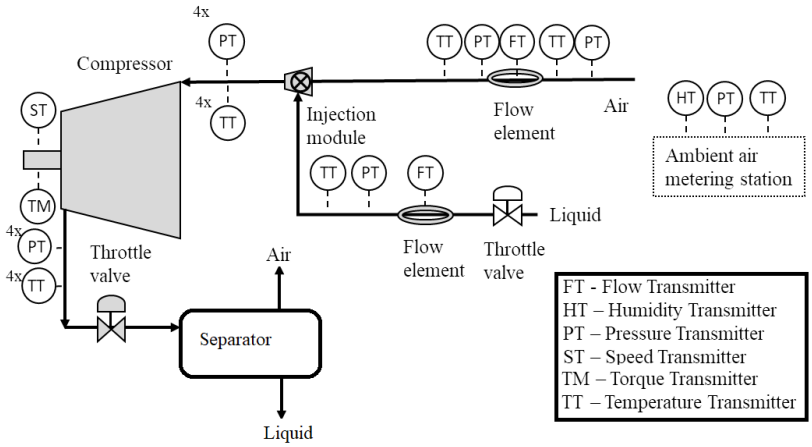

Figure 8 NTNU test rig process flow diagram

Table 1 - Test rig operational range [23]

Design parameter	Data
Suction conditions	Atmospheric
Test fluids	Air/water
Air-flow range	0-3 kg/s
Water-flow range	0-5 kg/s
GVF range	99.93-100%
GMF range	40-100%

Pipe sections in PMMA (acrylic) give visual access to the main sections of the compressor inlet piping. At the front of the diffuser (shroud side), four large PMMA windows provide visual access from the impeller outlet to the outlet scroll. In the cross-support of the PMMA windows, slots for the installation of various instrumentation are implemented along the radial direction. The compressor section is split in the diffuser plane to allow integration of the PMMA section in the scroll. This ensures visual access radial to the whole width of the diffuser. The locations of the PMMA windows are shown in Figure 9 and the main compressor and loop dimensions are given in Table 2.

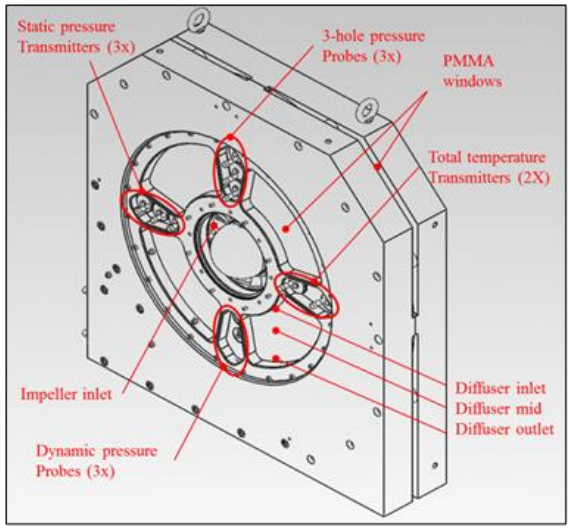

Figure 9 Compressor section

Table 2 - Main compressor dimensions

Parameter	Data
Impeller design	Shrouded 3D design with inducer and splitter vanes
Impeller tip width	20 mm
Impeller outlet diameter	400 mm
Diffuser	vaneless
Diffuser width	20 mm
Diffuser ratio	1.7
Inlet hub diameter	250 mm
Inlet pipe diameter	250 mm
Outlet pipe diameter	200 mm
Volute	Circular central symmetrical

An orifice meter upstream of the injection module measures the air volume flow and electromagnet flowmeters measure the water volume flow. Pressure and temperatures are measured at compressor suction (downstream of the injection point) and compressor discharge. Pressure and temperature measurements at suction and discharge are in

accordance with ASME PTC10, i.e., four pressure and four temperature probes. Furthermore, a torque meter measures the compressor torque and power. At the discharge, the fluid passes a throttle valve and finally, the fluid enters a separator. The V-ball discharge throttle valve is used to fix the compressor inlet volume flow and the liquid throttle valve to tune gas mass fraction (*GMF*). The data acquisition system for the test rig is National Instruments' PXI solution, which allows a high synchronous sampling rate. Further test rig details have been outlined by Hundseid and Bakken [23]. Figure 10 depicts the inlet section and compressor in the test rig.

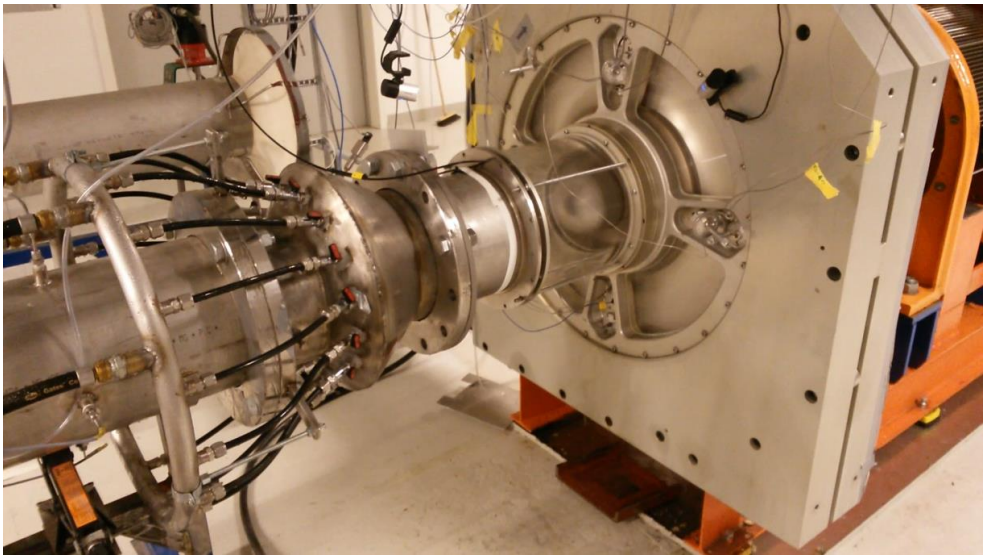

Figure 10 Compressor test facility

The use of inert fluids, i.e., water and air at ambient conditions enables several advantages for investigation and implementation of new compressor technology:

- Testing can be considered safe, as no dangerous or toxic emissions are associated with it. However, focusing on safety relating to machine integrity is of paramount importance.
- The design and implementation of modifications are quick and low cost compared to modifications inside a hydrocarbon test facility. This is because low pressure and temperature class equipment are used and no ATEX requirements are necessary.
- Instrumentation of low uncertainty is available at a reasonable price.
- The use of inert fluids, such as water and air, simplifies the PVT calculations, since the composition of the faces is well established and little phase transition occurs, the physical properties of the faces are known with low uncertainty and good control of the flow rate of the phases is achieved.

The above-mentioned advantages make the testing with inert fluids at ambient conditions an obvious choice for testing wet gas compressor designs in the first phase of concept development. However, clear challenges with regards to realistic behaviour compared to hydrocarbon multicomponent fluids at high pressures must be considered. Parameters, such as the density ratio between liquid and gas, surface tension between liquid and gas, and the viscosity of the phases are not comparable between the inert conditions and the realistic high-pressure hydrocarbon conditions. Also, the phase transition throughout the stage is very low in ambient water air conditions compared to realistic hydrocarbon gas and liquid compression.

The NTNU compressor consists of a single impeller with an axial inlet, this contrasts with conventional centrifugal compressors in the oil and gas industry that are multistage machines with radial inlets and outlets. This has consequences for the comparison of results between water/air and realistic conditions. Axial inlet compressors typically have a higher efficiency than the radial inlet and the loss associated with the radial inlet is not exposed. The horizontal axial inlet easily leads to segregated flow causing liquids to only impact the bottom part of the impeller eye. Furthermore, by only testing a single impeller, no impeller matching can be investigated.

3.2 K-Lab Test Facility

The K-lab test facility is located inside the Kårstø processing plant on the west coast of Norway. K-lab is one of Equinor's research and technology laboratories and serves as a hub for the full-scale testing and qualification of process equipment.

The K-Lab test facility consists of two multiphase full-scale test loops, named the VGII and SST, respectively. The VGII has a 2.8 MW and the SST loop has a 12 MW variable speed drive. Data presented in this thesis were collected from the VGII loop. Figure 11 shows a simplified process flow diagram (PFD) of the VGII multiphase test loop.

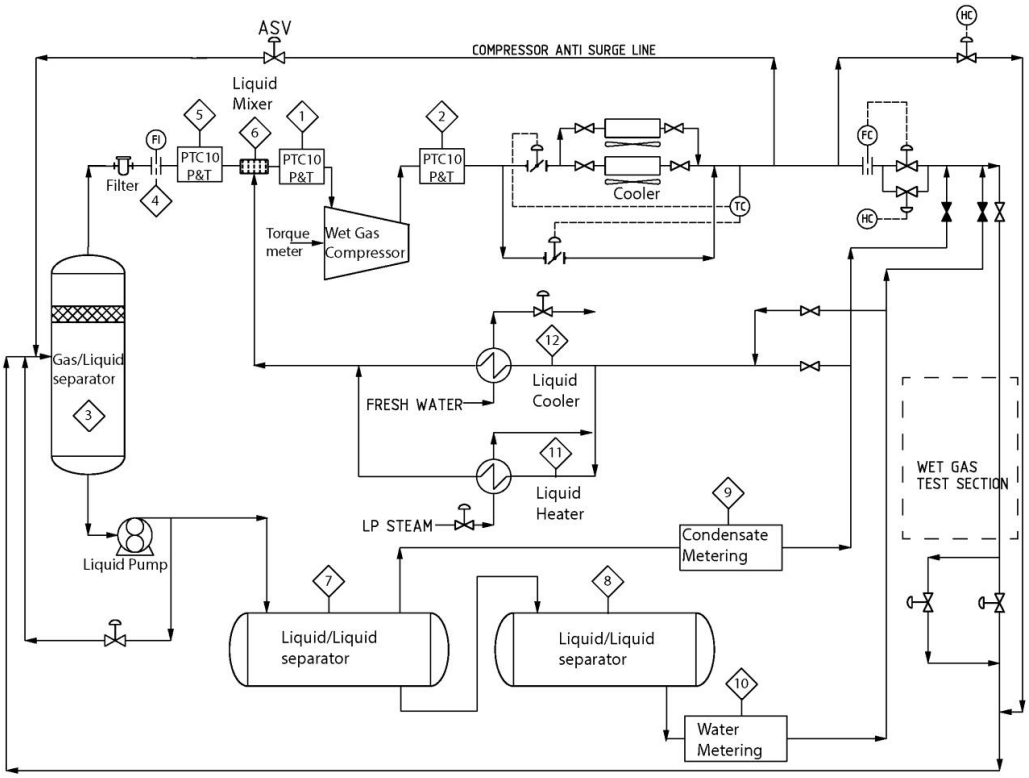

Figure 11 VGII - K-Lab wet gas test loop

It is a closed loop typically operated with a mixture of water, oil (condensate) and natural gas. Some important design parameters for the compressor section are given in Table 3 and available test fluids are listed in Table 4

Table 3 Design parameters for the K-Lab loops

Design parameters	**VGII**
Flowrate [Am^3/h]	6000
Liquid flow rate [Am^3/h]	0-150
Design pressure suction [Bar]	149
Design pressure discharge [Bar]	149
Design temperature suction Min/Max [°C]	-46/90
Design temperature discharge Min/Max [°C]	-46/130
GVF [-]	1-0.95
GMF [-]	1-0.7

Table 4 Available test fluids at K-Lab

GAS
Hydrocarbon rich gas
Hydrocarbon sales gas
Nitrogen

LIQUID
Hydrocarbon condensate from Kårstø gas processing plant
Light oils from marked, to fit specific test matrix
Fresh water
Saline water
Monoethylene glycol (MEG)
Triethylene glycol (TEG)

The following is a brief description of the loop configuration as it was when data presented in this thesis was collected. The gas was separated from the liquid in the gas/liquid separator (3) and the gas flow was measured in an orifice meter (4) upstream of the liquid mixer. Liquids were pumped from the bottom of the gas/liquid separator and into the liquid/liquid separation (7 and 8) system where water and oil were separated. Water and oil amounts were metered in liquid metering stations (9 and 10) using Coriolis flowmeters. The liquids were further conditioned by the liquid heater/cooler setup (11 and 12) before entering the liquid mixer (6) upstream of the wet gas compressor. Pressure and temperature measurement locations containing four pressure and four temperature probes, as described in the ASME PTC 10 code, were installed at three locations: Upstream liquid mixer (5) at compressor inlet (1) and compressor discharge (2). These stations are indicated as PTC10 boxes in the PDF. A torque meter was installed during the wet gas compressor test, ensuring accurate power measurements.

The two-impeller compressor, for which test data are reported in this thesis, was equipped with specially designed internal instrumentation. This included:

- Pressure and temperature probes in the U-bend of the compressor.
- Pressure probes throughout the flow path.
- Level transmitters at several locations monitor liquid levels in the machine.
- Temperature and flow measurements on the oil system, to allow for lube oil loss calculations.

The pressure and temperature probes in the U-bend were intended for performance calculations of the first impeller. However, the accuracy of these instruments did not meet the required quality to allow for such calculations, thus no data of sufficient quality could be obtained for the evaluation of the first impeller performance.

3.2.1 PVT calculations

In multiphase test loops operating with real hydrocarbon fluids, a system for PVT calculations that can handle phase transitions and calculate phase properties is of crucial importance. The following is a description of the main principles of the PVT calculations used for analysing the wet gas compressor performance results.

A system for maintaining a timeline budget of all components added to or removed from the inventory has been implemented at the K-Lab test facility, it is called the loading system and is of crucial importance for ensuring the quality of the thermodynamic calculations throughout the test campaigns.

As fluids are circulated in the test loop, the basis for the loop PVT calculation is the main separator PT-flash (flash calculation of a known composition at a given pressure and temperature). The main separator PT-flash applies the composition obtained from the total loop inventory at the pressure and temperature of the gas/liquid separator (3) seen in

Figure 11. The resulting outputs are phase compositions as well as mixture and phase properties. The resulting gas phase composition is extracted and a PT-flash of this fluid is calculated on the orifice metering station (4) conditions. The resulting properties are used to calculate the gas flow in accordance with the ISO 5167-2. Furthermore, this gas fluid is flashed upstream of the liquid mixer indicated by the PTC10 box (5) in Figure 11. The liquid phases resulting from the gas/liquid separator PT-flash are extracted and separated by a PT-flash under liquid/liquid separator conditions (7). The resulting oil and water phases represent fluids entering the liquid metering stations (9 and 10) where the flow rates are established. At the liquid mixer (6) upstream of the compressor, the resulting oil, water and gas phases are mixed according to the flow rates obtained from the metering stations. A PT-flash is performed on this mixture at the location upstream of the compressor indicated by the PTC10 box (1) in Figure 11. Eventually, a PT-flash is performed for the same mixture at the conditions at the PTC10 box (2) at compressor discharge. As the liquid is injected upstream of the compressor, the temperature ratio over the compressor is reduced, thus uncertainties increase for wet gas performance results that are based purely on thermodynamic calculations. Therefore, the PTC10 flash downstream of the compressor was also calculated based on compressor power input obtained from a torque meter and the total fluid mass flow by performing a PH-flash at discharge conditions.

PVT calculations are based on the PVTsim simulation program, using the SRK Peneloux(T) equation of state, and the viscosity model based on corresponding states principle (CSP). A more comprehensive description of the equation of state (EOS), mixing rules, and flash calculations can be found in Appendix A.

3.2.2 K-Lab facility Summary

The use of realistic fluids, i.e., hydrocarbon gas, hydrocarbon liquids and water at high pressure and realistic temperatures for testing compressor technology is more expensive compared to inert ambient testing. However, testing at realistic conditions is essential for the qualification of equipment as well as the theoretical foundations. Some important aspects are:

- Full-scale testing can reveal scaling effects that are not found during prototype testing
- Similarity conditions for multiphase equipment can be impossible to achieve in water/air ambient test conditions, thus full-scale testing at realistic conditions with hydrocarbon gas, hydrocarbon liquid, and water are necessary to achieve realistic results.
- The use of realistic fluids, pressures and temperatures gives realistic fluid and thermodynamic behaviour of the compressor. This includes realistic phase transitions, density ratios between liquids and gas, viscosities, etc. Realistic thermodynamic properties at realistic operating speeds will also give realistic dimensionless numbers such as Mach number, Reynolds number, specific volume ratios, Stokes number, etc. These are examples of parameters that are necessary to achieve similarity conditions.
- Systems testing: A compressor must be considered together with its system. The system includes equipment, such as motor, VSD, gearbox, and utilities, such as seal gas conditioning skid, seal gas panel, lube oil system or magnetic bearing system depending on the design configuration. To qualify a compressor for wet gas operation, full-scale systems testing provides proof of technology before final implementation into operation.

Testing under actual conditions is typically done at the later stages of technology qualifications, i.e., before the first implementation into operation. However, realistic testing is challenging due to the high cost caused by the comprehensive engineering, procurement and construction phase. Cost-increasing elements are ATEX requirements, safety systems, such as overpressure protection, blow down, emergency shutdown and process shutdown systems.

4 METHOD DESCRIPTION FOR WET GAS COMPRESSOR ANALYSIS

This chapter summarizes the methods used in this thesis. This includes methods used to investigate the similarity theory and its validity for wet gas, and methods used to generate a novel model for wet gas performance. Furthermore, the methods used for uncertainty investigation of wet gas performance parameters and methods used to evaluate how fouling affects wet gas compressor performance.

4.1 Similarity analysis for wet gas centrifugal compressor

As regards wet gas compressors, there is currently limited knowledge on how the performance will shift due to changing inlet conditions. Therefore, the vendors are unable to estimate performance for a specific wet inlet condition a priori. This gives rise to challenges both for the design and operational phase. Furthermore, no internationally established standards, such as the dry gas standards ASME PTC10 [2] or ISO 5389 [3], exist for performance evaluation of wet gas compressors. The dry gas standards are based on the theory of model testing as outlined in ASME PTC 19.23 [24], which in turn is largely based on the Buckingham π theorem for dimensional analysis [25]. The dry gas standards allow for two types of tests: Type 1 test (same operating conditions in specified and test point), and Type 2 test (different operating conditions in specified and test point, where speed is selected to target for similarity conditions). To ensure similarity, permissible deviations between specified and test conditions in several parameters are required. These are specific volume ratio, flow coefficient, Machine Mach number, and Machine Reynolds number. Type 2 tests are the most common performance test for dry compressors and are usually conducted at the manufacturer's premises. Results obtained from Type 2 tests are back-calculated to specified (guarantee) conditions, assuming similarity.

Several of the requirements given in the dry gas standards are challenging to apply to wet conditions. Thus, multiple aspects of the similarity theory need to be addressed to evaluate if and how it can be applied for wet gas performance evaluation:

- Can kinematic similarity parameters such as the ones used for dry gas be used also for wet gas compressor performance evaluation?
- What dynamic similarity parameters should be used to wet gas, and how should they be defined?
- Is Type 2 testing possible for wet gas compressors?

The method used to investigate similarity theory in the context of wet gas compression was mainly theoretical reasoning. By revisiting the dry gas similarity theory for turbomachinery, the main assumptions could be found and the limitations for the adaptation to wet gas compressors could be identified. In addition to the theoretical considerations, some simulations were performed to investigate how the proposed definitions of the Stokes and Weber number would vary for varying wet gas operating conditions. The PVT simulation software PVTsim nova was used to generate the thermodynamic data.

The basic requirements for similitude are outlined in ASME PTC 19.23[24], which is largely based on the Buckingham π theorem for dimensional analysis [25]. The similarity requirements are given by:

Geometric similarity: The model and prototype must be geometrically similar. This means that the model is a scaled version of the prototype.

Kinematic similarity: This requires the motion through the model and prototype to be similar. This means that the ratio of velocities and accelerations between prototype and model need to be constant, thus

$$\frac{v_{X,Y,Z}}{v_{x,y,z}} = constant \tag{32}$$

and

$$\frac{A_{X,Y,Z}}{A_{x,y,z}} = constant \tag{33}$$

Here, X, Y, X and x, y, z denote corresponding positions in the prototype and model respectively.

Dynamic similarity: Forces acting on corresponding masses passing through the system are similar in the model and the prototype, thus

$$\frac{\left(\frac{F}{m}\right)_{X,Y,Z}}{\left(\frac{F}{m}\right)_{x,y,x}} = constant \tag{34}$$

Examples of parameters that must be similar for dynamic similarity to apply are dimensionless numbers, such as the Reynolds number, Weber number, Mach number, etc.

Since the test and prototype compressor is the same unit/machine in ASME PTC10 and ISO5389 type performance tests, compressor geometric similarity is satisfied. This also holds for wet gas compressors. Before investigating kinematic similarity for wet gas, a review of the dry gas kinematic similarity is performed.

4.1.1 Kinematic similarity for dry gas compressors

For kinematic similarity as given in Eq.(32) and Eq.(33) to be true, similar velocity triangles under specified and test conditions are required. Considering the impeller velocity triangles, requirements for the impeller eye and impeller tip similarity can be evaluated.

Starting at the impeller eye, the requirement for similar triangles can be given as:

$$\left(\frac{C_{eye}}{U_{eye}}\right)_t = \left(\frac{C_{eye}}{U_{eye}}\right)_{sp} \tag{35}$$

Here, C_{eye} is the axial flow at the impeller eye. By applying the continuity equation $C_{eye} = Q_{eye}/A_{eye}$, and the relations $U_{eye} = 2\pi r_{eye}N$ for impeller eye peripheral speed, the following result is obtained:

$$\left(\frac{\frac{Q_{eye}}{A_{eye}}}{2\pi r_{eye}N}\right)_t = \left(\frac{\frac{Q_{eye}}{A_{eye}}}{2\pi r_{eye}N}\right)_{sp} \tag{36}$$

Which gives the following impeller eye similarity relation.

$$\left(\frac{Q_{eye}}{N}\right)_t = \left(\frac{Q_{eye}}{N}\right)_{sp} \tag{37}$$

Recalling the expression for the flow coefficient $\phi = \frac{4Q}{\pi D^3 N}$, it becomes clear that the following expression is also an impeller eye similarity requirement:

$$\phi_t = \phi_{sp} \tag{38}$$

Next, looking at the requirement for similar velocity triangles at the impeller tip, assuming the angle of the relative velocity to be given by the impeller discharge blade angle and this velocity angle to be equal between test and specified conditions, a similar expression can be given:

$$\left(\frac{Q_{tip}}{N}\right)_t = \left(\frac{Q_{tip}}{N}\right)_{sp} \tag{39}$$

By combining these expressions for the impeller eye and tip, the following is the case:

$$\frac{N_{sp}}{N_t} = \frac{Q_{eye_{sp}}}{Q_{eye_t}} = \frac{Q_{tip_{sp}}}{Q_{tip_t}} \tag{40}$$

Substituting $Q = \dot{m}v$ this gives:

$$\frac{N_{sp}}{N_t} = \frac{\dot{m}_{sp}v_{eye_{sp}}}{\dot{m}_t v_{eye_t}} = \frac{\dot{m}_{sp}v_{tip_{sp}}}{\dot{m}_t v_{tip_t}} \tag{41}$$

Which gives

$$\left(\frac{v_{eye}}{v_{tip}}\right)_{sp} = \left(\frac{v_{eye}}{v_{tip}}\right)_{t} \tag{42}$$

In summary, the deduced kinematic similarity requirements for dry gas are:

$\phi_t = \phi_{sp}$ and $\left(\frac{v_{eye}}{v_{tip}}\right)_{sp} = \left(\frac{v_{eye}}{v_{tip}}\right)_{t}$.

4.1.2 Kinematic similarity for wet gas compressors

For a wet compressor, where liquids are introduced through the inlet duct, reoriented and led towards the impeller eye, it is reasonable to assume that the liquid droplets will not follow the same trajectory as the gas. One can argue that this reorientation of the mixture causes liquid and gas to hit the impeller eye at different angles and, due to phase slip, at different velocities. The velocity triangles, especially for the liquid droplets, will also vary at different impeller eye locations.

Phase coupling should also be considered, as both momentum coupling and mass coupling (due to evaporation) will affect the droplet and gas flow field, hence also affecting the velocity triangles. Momentum coupling effects will increase with decreasing *GVF*.

Two important parameters for describing the ability of droplets to follow the gas flow field are the Stoke number, St, and the liquid-gas density ratio. Several authors [9, 22] have proposed the relevance of the density ratio.

The simplified analysis above illustrates how the complexity regarding determining kinematic similarity increases when introducing wet gas into the compressor. For wet gas kinematic similarity to be valid at the impeller eye, one possible approach could be to include additional requirements to the dry gas requirements given by Eq.(35) to Eq.(38). Such requirements could include restricting the Stokes number, liquid/gas density ratio, etc., to specified limits of deviation between test conditions and specified conditions.

Furthermore, looking at the impeller tip, when applying the same reasoning as with the impeller eye, it can be argued that the resulting velocity triangles for the gas and liquid phase will not be equal, hence additional requirements are also necessary for impeller tip kinematic similarity. Extending this reasoning even further, two-phase flow can be expected to complicate the flow field throughout the compressor; hence the impeller eye and tip kinematic similarity might not be sufficient requirements for similar flow fields throughout the machine.

In this context, the effect of altered velocity triangles on the efficiency of the compressor should also be mentioned. As the liquid and gas phases have different angles of attack on the impeller, the optimum angle for both phases cannot be met at the same time, hence two-phase flow will have a negative impact on compressor efficiency.

4.1.3 Dynamic similarity for wet gas compressors

Assuming there is a method of determining kinematic similarity for wet gas compression, the next step is to find relevant dimensionless parameters to achieve dynamic similarity. Candidates for such parameters are:

- Machine Mach number
- Reynolds number
- Droplet Reynolds number
- Stokes number
- Weber number

Definitions of these parameters are given in Chapter 2. The challenge that arises when attempting to use such numbers for wet conditions is that the required properties are not uniquely defined or not easily obtainable. Speed of sound, density, and viscosity are examples of properties not uniquely defined for wet flow. Several equations for the speed of sound have been suggested for wet gas [26, 27] and the homogeneous density can potentially be applied to gain a good approximation and several dynamic viscosities for multiphase flow have been proposed [12, 28, 29]. Furthermore, several of the

variables will vary throughout the machine. This means that significant research is required to find suitable definitions for wet gas compression.

4.1.4 Suggestion for machine Stoke and Weber numbers

Since most compressor performance measurements are flange to flange measurements and recalling how the machine Reynolds number is defined, it is tempting to define a Machine Stokes number and a Machine Weber number similarly. One attempt could be to define the Stokes number as

$$Stm = \frac{\rho_D d_D^2 U_2}{18\mu_G\, b} \tag{43}$$

Here, all the parameters could be assumed to be at the compressor inlet (this would of course require knowledge of these magnitudes), the characteristic length, b of the system is chosen to be the first stage impeller exit width and U_2 can be chosen as the first impeller tip speed.

Furthermore, a Machine weber number could be defined as

$$Wem = \frac{\rho_G U_2^2 d_D}{\sigma_D} \tag{44}$$

Here the parameters could also be defined at inlet conditions and U_2 chosen to be the first impeller tip speed.

4.2 Creating a model for the wet gas hydrocarbon centrifugal compressor test results

Depending on reservoir depletion, wet well stream compressors will experience a gradual shift in inlet pressure and fluid behaviour. Therefore, a major challenge both to designers and operators of wet gas compressors is understanding the impact of changing operating conditions, such as gas mass fraction and density ratio, on performance. Currently, the similarity theory is limited for wet applications and cannot predict which wet conditions are comparable. Precise models that can predict wet gas performance are therefore of great interest and will be important for project development and later for operational organizations.

A full-scale wet gas test was conducted on a two-impeller centrifugal compressor at K-Lab as part of a technology qualification program. The test was conducted under realistic conditions i.e., realistic hydrocarbon composition, pressures, and temperatures. A broad range of suction pressures was investigated with a gas mass fraction ranging from 0.7 to 1.0. Based on these results, a novel approach for modelling wet performance at varying inlet conditions was developed. The basis for the model was to merge key dimensionless parameters into a single wet variable that allows performance parameters to be given as a function of flow coefficient and this new variable. The test data used to develop the model cover significant variations in gas-mass fraction, fluid density ratio and Mach number. A comprehensive test campaign was conducted as part of the technology qualification with compressor speeds ranging between 8807- and 13210 rpm, and a suction pressure between 20 and 110 bar. However, in this work, the focus is on wet performance data obtained as part of the compressor mapping. The latter part of the test campaign included a fouling test. Any test points taken after the onset of the fouling test are associated with performance degradation and are thus removed from the dataset.

It is widely known that the gas mass fraction, *GMF*, strongly affects the wet performance of centrifugal compressors. However, on its own, the *GMF* does not completely describe the effect. To illustrate this Figure 12 and Figure 13 show normalized polytropic efficiency vs normalized flow coefficient for two of the curve sets, namely 125-90-HC and 55-90-HC, as given by the test matrix (Table 8). The curve set name convention is indicated by: percent of design pressure – per cent of design speed – liquid type. It is clear from this figure that the efficiency of both curve sets is strongly affected negatively by increasing liquid content. Furthermore, the 55-90-HC curve set is more affected by the increasing liquid amount than the 125-90-HC curve set. A major difference between these curve sets is the suction pressure, hence the density ratio between liquid and gas also differs. The liquid to gas density ratio for curve sets were approximately 12 and 30 where higher pressure gives a lower density ratio.

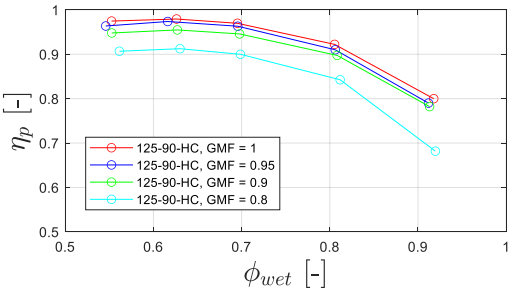

Figure 12 Normalized polytropic efficiency vs normalized flow coefficient for curve set 125-90-HC.

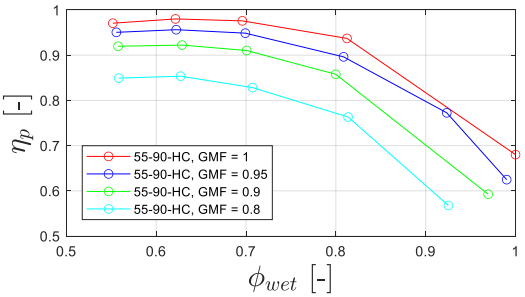

Figure 13 Normalized polytropic efficiency vs normalized flow coefficient for curve set 55-90-HC

As the performance is impacted more strongly for larger density ratios when comparing curves of the same *GMF*, the density ratio is obviously one parameter of interest when trying to model wet gas performance. Furthermore, other parameters also contribute to the shift in wet performance and were investigated.

To model the change in wet performance for different operating conditions, the starting point was the notion that the wet-polytropic head coefficient and polytropic efficiency could be modelled by polynomial surfaces represented by the flow coefficient, and a new wet variable Γ. The third-degree polynomial surface was chosen for the polytropic head coefficient and is given by an equation of the form:

$$\mu_p(\phi_{wet}, \Gamma_{\mu_p}) = p_{00} + p_{10}\phi_{wet} + p_{01}\Gamma_{\mu_p} + p_{20}\phi_{wet}^2 + p_{11}\phi_{wet}\Gamma_{\mu_p} + p_{02}\Gamma_{\mu_p}^2 + p_{30}\phi_{wet}^3 + p_{21}\phi_{wet}^2\Gamma_{\mu_p} + p_{12}\phi_{wet}\Gamma_{\mu_p}^2 + p_{03}\Gamma_{\mu_p}^3 \quad (45)$$

and the polytropic efficiency is given by:

$$\eta_p(\phi_{wet}, \Gamma_{\eta_p}) = p_{00} + p_{10}\phi_{wet} + p_{01}\Gamma_{\eta_p} + p_{20}\phi_{wet}^2 + p_{11}\phi_{wet}\Gamma_{\eta_p} + p_{02}\Gamma_{\eta_p}^2 + p_{30}\phi_{wet}^3 + p_{21}\phi_{wet}^2\Gamma_{\eta_p} + p_{12}\phi_{wet}\Gamma_{\eta_p}^2 + p_{03}\Gamma_{\eta_p}^3 \quad (46)$$

Where ϕ_{wet} is the flow coefficient, Γ_{μ_p} is the wet variable for the polytropic head coefficient model, Γ_{η_p} is the wet variable for the polytropic efficiency model, and the p's are the regression coefficients for the polynomial surface of degree 3 in ϕ_{wet} and degree 3 in Γ_{μ_p} and Γ_{η_p}.

Furthermore, it was suspected that the wet variable Γ can be represented as a function of important dimensionless parameters such as *GMF*, density ratio, and possibly other variables such as the viscosity ratio between the gas and liquid phase, etc. The general form of the wet variable Γ selected was given by the equation

$$\Gamma(X_1, X_2, \dots, X_n) = X_1^{a_1} X_2^{a_2} \dots X_n^{a_n} \quad (47)$$

where $X_1, \dots, X_n$ are dimensionless variables and $a_1, \dots, a_n$ are constants. To establish the constants $a_1, \dots, a_n$, that generate the best models in Eq.(45) and Eq.(46), the MATLAB optimization function fmincon was used. The objective function for the optimization was based on maximizing the goodness of fit variable R^2. Figure 14 illustrates an example of the modelled normalized polytropic head coefficient as a function of the normalized flow coefficient and the wet variable defined by Eq.(47), and

Table 5 shows examples of different choices of the wet variable Γ that were investigated. As can be seen in Figure 14, the model is represented by the surface plotted together with the datapoints for all the curve sets. One advantage of the proposed method is that it allows for visualization of the model in such 3D plots.

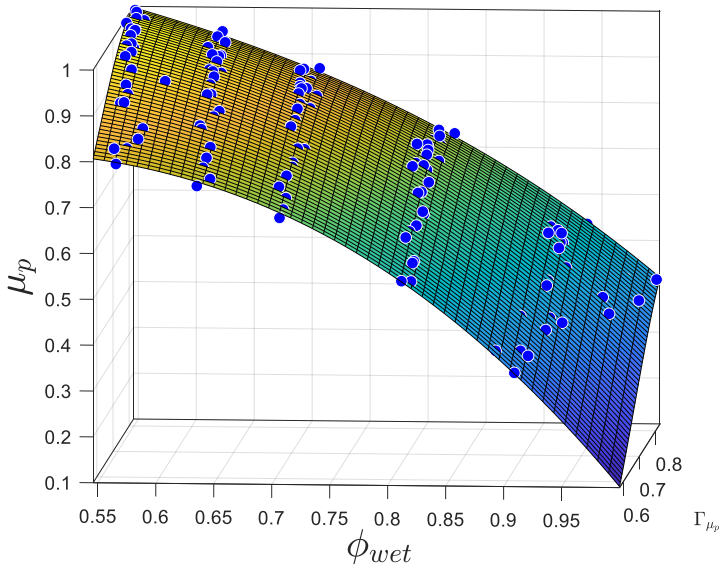

Figure 14 Example of normalized polytropic head coefficient plotted against normalized flow coefficient and the wet variable Γ. The model is represented by the surface shown in the plot.

Table 5 Examples of different variants of the wet variable Γ_{μ_p} that have been investigated.

Predicted variables	Wet variable Γ_{μ_p}
μ_p, η_p	GVF^{a_1}
μ_p, η_p	GMF^{a_1}
μ_p, η_p	$\left(\frac{\rho_m}{\rho_g}\right)^{a_1}$
μ_p, η_p	$\left(\frac{a_m}{a_g}\right)^{a_1}$
μ_p, η_p	$GMF^{a_1} GVF^{a_2}$
μ_p, η_p	$\left(\frac{\dot{m}_l}{\dot{m}_g}\right)^{a_1}\left(\frac{\rho_g}{\rho_l}\right)^{a_2}\left(\frac{\mu_l}{\mu_g}\right)^{a_3}$
μ_p, η_p	$GMF^{a_1} Ma_{wet}^{a_2}$
μ_p, η_p	$Ma_{wet}^{a_1}\left(\frac{\rho_m}{\rho_g}\right)^{a_2}$
μ_p, η_p	$Ma_{wet}^{a_1}\left(\frac{\rho_g}{\rho_m}\right)^{a_2}\left(\frac{\mu_m}{\mu_g}\right)^{a_3}$
μ_p, η_p	$LMF^{a_1}\left(\frac{\mu_l}{\mu_g}\right)^{a_2}\left(\frac{\rho_g}{\rho_l}\right)^{a_3}$
μ_p, η_p	$LMF^{a_1} LVF^{a_2}\left(\frac{\mu_l}{\mu_g}\right)^{a_3}$

4.3 Uncertainty and sensitivity analysis for wet gas compressor test results

When evaluating the performance parameters of a wet gas compressor, knowledge of the standard uncertainty of the results is of great importance. Therefore, the uncertainties of compressor performance parameters in a wet gas test loop were investigated. The VGII test loop (see Figure 11) was taken as the basis for the calculations. A simplified version of the loop was modelled. Both one wet and one dry case were investigated. The uncertainties were propagated through the whole wet gas test loop system by the Monte Carlo Method (MCM) and a sensitivity analysis were performed. This way, the total expanded uncertainties were established and from the sensitivity analysis, it was possible to investigate which input parameters had the greatest effect on the output parameters. The uncertainty results for SRK Peneloux(T) and PR78 Peneloux(T) EOS were documented and the effect of two different polar components models, namely the Huron-Vidal and Cubic-Plus-Association were investigated. This gives a comprehensive picture of which uncertainties can be expected for different compressor performance parameters. Furthermore, it illustrates what uncertainties can be expected resulting from measurement uncertainties and what can be expected from the choice of EOS.

4.3.1 Monte Carlo Method

The most recognized international standard for the evaluation of uncertainty is the Guide to the Expression of Uncertainty in Measurement (GUM) [30]. Another commonly used standard is the ASME PTC 19.1 Test Uncertainty [31]. In the GUM, propagation of uncertainty calculations is based on a first-order Taylor approximation of $\boldsymbol{Y = f(X_1, X_2, \dots, X_N)}$, where $\boldsymbol{Y}$ is the measurand and $\boldsymbol{X}$ is the input quantities to the functional relationship. The exception is for highly nonlinear systems where higher-order derivatives are required. Also, to correctly determine the coverage factor for the measurand, knowledge of the probability distribution of $\boldsymbol{Y}$ is required. As stated in Annex G.1.5 of the GUM: "If the functional relationship between Y and its input quantities is nonlinear and a first-order Taylor series expansion of the relationship is not an acceptable approximation, then the probability distribution of Y cannot be obtained by convolving the distribution of the input quantities. In such cases, other analytical or numerical methods are required." Such a numerical method is outlined in GUM Supplement 1 [32], where the Propagation of Distributions using a Monte Carlo Method (MCM) is given. For a complicated system, such as the wet gas compressor system simulated here, it is clear that a Monte Carlo Method (MCM) is right for analyzing the propagation of uncertainty for the wet gas compressor system analyzed.

A simulation model was developed for the investigation. The simulation was written as a MATLAB code and data was passed to and from PVTsim Nova 4 via the Open Structure API, where all flash calculations were performed. The MATLAB code, including PVTsim database files used to produce the results, are freely available at [33]. The modelled system is illustrated in Figure 15 and can be regarded as a simplified model of the VGII loop shown in Figure 11.

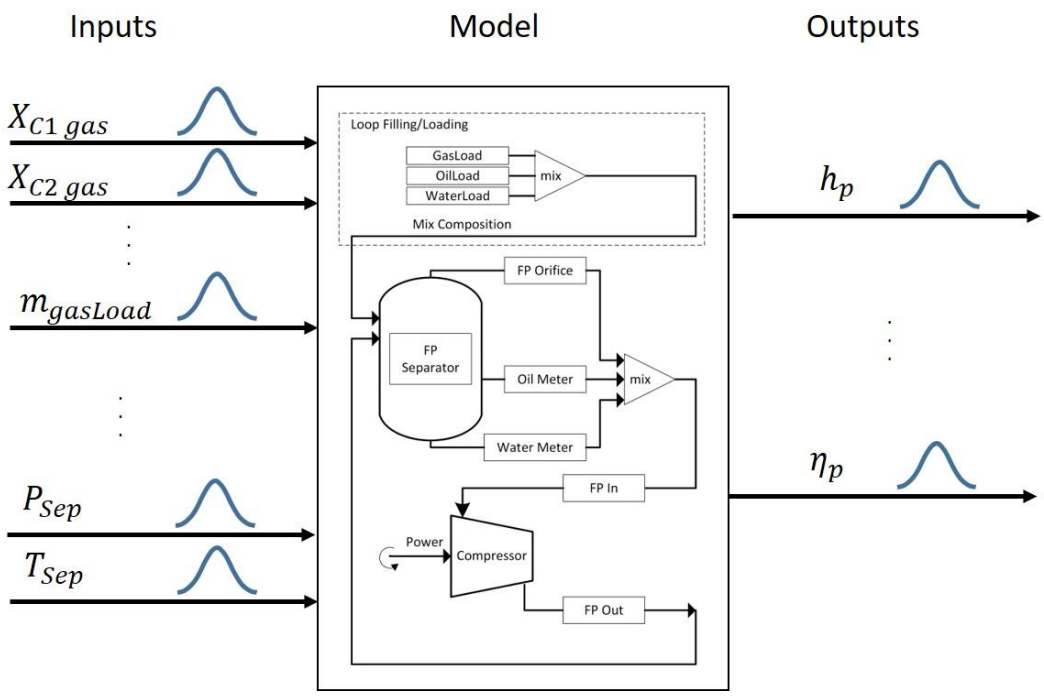

Figure 15 Illustration of the modelled system

A set of input parameters was selected for both the wet and dry cases. From the input parameters and their designated probability density functions, random samples were pulled and passed to the model.

One wet and one dry case were investigated, and for each case, the calculations have been conducted for both SRK Peneloux(T) and PR78 Peneloux(T) equations of state. The Peneloux(T) was used, as it is known to give better estimates for liquid density. Further, for each choice of EOS, the calculations were conducted using both the Huron and Vidal (HV) and Cubic-Plus-Association (CPA) polar components model. The combinations used for PVTsim Nova setup are listed in Table 6. For each case listed in Table 6, the MCM was conducted for 10,000 sets of randomly sampled input parameters.

Table 6 PVTsim Nova setup for cases

	EOS	Polar Components	Viscosity Model
Wet case Setup 1	SRK Peneloux(T)	HV	CSP
Wet case Setup 2	SRK Peneloux(T)	CPA	CSP
Wet case Setup 3	PR78 Peneloux(T)	HV	CSP
Wet case Setup 4	PR78 Peneloux(T)	CPA	CSP
Dry case Setup 1	SRK Peneloux(T)	HV	CSP
Dry case Setup 2	SRK Peneloux(T)	CPA	CSP
Dry case Setup 3	PR78 Peneloux(T)	HV	CSP
Dry case Setup 4	PR78 Peneloux(T)	CPA	CSP

For the random sampling of compositional data, another scheme is required compared with other input parameters. Misinterpretations of correlations in compositional data have long been a disputed subject in the field of geology, and the source of the problem is as explained by J. Aitchison [34]: "The difficulty arises because a basis or open vector of uncorrelated positive quantities $\boldsymbol{x_1, \dots, x_{d+1}}$ leads to a composition or closed vector of proportions $\boldsymbol{y_i = x_i/(x_1 + \cdots + x_{d+1})}$ $\boldsymbol{(i = 1, \dots, d + 1)}$ which are necessarily correlated."

A problem of this type was met in the loop simulations, as random compositional data for the Monte Carlo simulations had to be sampled. Two different approaches were used for estimating the uncertainties of compositions arising from gas chromatographs, one method for the gas and another for the condensate.

Random sampling of compositional data for the gas: The standard deviation of compositional data of the rich gas was calculated using $\boldsymbol{s_R = e^{-4.28+0.715\ln(x_i)}}$, (found in ISO 6974-3 [35]). The methane standard deviation was then set to 0. The random values for all components, except methane, were generated using the normal distribution with a molar fraction as expected values and $\boldsymbol{s_R}$ as standard deviation. After generating $\boldsymbol{n}$ random values, the results were normalized. This results in standard deviations comparable with the values given in ISO 6974-3 for all components including methane. This can be called the conventional approach [36].

Random sampling of compositional data for the oil/condensate: The oil/condensate composition uncertainties were estimated based on statements from a laboratory and repeated condensate samples taken at K-lab. The perturbations were performed for all components, assuming zero covariance, and normalized after perturbation. This method gives negative covariance between the dominant component, C10+, and all other components.

4.3.2 Sensitivity analysis

While the quantitative total expanded uncertainties were obtained from the MCM, a sensitivity analysis (SA) provides additional information about how uncertainties in the output of the model can be apportioned to different sources of uncertainty in the model input. When the sensitivities are established, this can help direct the effort for which input uncertainties should be reduced if one aims to reduce the overall uncertainty of the output. It is therefore always advisable to perform an SA together with the uncertainty analysis. Sensitivity analysis can be divided into two groups, namely local and global methods. If a model is given by the function $\boldsymbol{y = f(x)}$, where $\boldsymbol{x = [x_1, x_2, x_3, \dots, x_k]}$ are the input parameters, the local sensitivity is given as the partial derivative of the model with respect to one of the input variables at a specific location, namely $\boldsymbol{\theta = \partial y / \partial x_i}$ [37]. The local method is in principle only valid for linear models and does not account for any covariance in the input variables. On the other hand, global methods give sensitivity over the total input parameter space. In this work, the global method of scatter plots, including correlations, was performed, but the main analysis was based on the sigma-normalized derivatives. The sigma-normalized derivatives are given as [38]:

$$\theta_{x_i}^{\sigma} = \frac{\sigma_{x_i}}{\sigma_y}\frac{\partial y}{\partial x_i} \tag{48}$$

Here, $\boldsymbol{\sigma_{x_i}}$ is the standard deviation of the population input $\boldsymbol{x_i}$, and $\boldsymbol{\sigma_y}$ is the standard deviation of the population output y. Note that the empirical standard deviations $\boldsymbol{s_{x_i}}$ and $\boldsymbol{s_y}$ were used as input to equation 48. The sigma-normalized derivatives $\boldsymbol{\theta_{x_i}^{\sigma}}$ have the property that the sum of its squares should add to unity for a linear system [38]

$$\sum_{i=1}^{k}\left(\theta_{x_i}^{\sigma}\right)^2 = 1 \tag{49}$$

One important feature of the local method for compositional data is that a step-change in one component leads to a change in all other components after normalization, and a step-change in a dominant component, say methane in natural gas, will be reduced dramatically after normalization. If a gas consists of 90% methane and a 1% step is performed, the resulting step size after normalization will be around 0.1%. For this reason, the step size after normalization was used to calculate the partial derivatives $\boldsymbol{\theta = \frac{\partial y}{\partial x_i}}$, which were used to establish sigma-normalized derivatives.

4.4 Fouling effects on wet gas centrifugal compressor performance

As mentioned earlier, a prerequisite for the successful implementation of subsea wet gas compressors is high reliability. Therefore, knowledge of possible failure modes is important. The detrimental effect of fouling on wet gas performance was observed as part of fouling testing at K-Lab, as mentioned in section 4.2. Therefore, an investigation of the effect in controlled conditions at NTNU was initiated. A test campaign was conducted to investigate the effect of fouling in both wet and dry conditions. The results documenting these effects are presented together with a proposed method for correcting the effects of fouling between dry and wet conditions.

Compressor operating experiences show several challenges related to deterioration: some to internal wear, i.e., labyrinth clogging, material pitting and deformation and others to internal flow channel fouling. Depending on the application and

operating conditions, the fouling deposits may vary from soft sticking 'glue' to a hard-shell cover. Roughness varies considerably between the various fouling cases. Representative cases are given in the figures below. Figure 16 shows the sticky fouling formed on a natural gas compressor. This compressor was fouled due to the carry-over of liquid hydrocarbons from the suction separator during operation at the Åsgard field, as the lighter components boiled off, the heavy hydrocarbon components were deposited on the compressor internals. Figure 17 shows fouling deliberately produced during the wet gas compressor test campaign at K-Lab. This deposit is pure iron carbonate precipitated during water evaporation through the compressor.

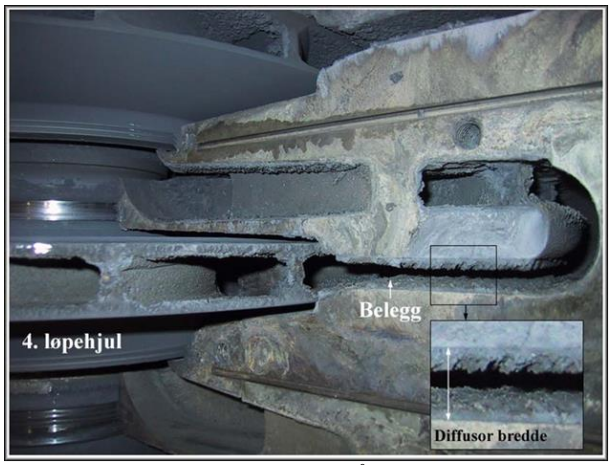

Figure 16 Impeller and diffuser on Åsgard compressor fouled during operation

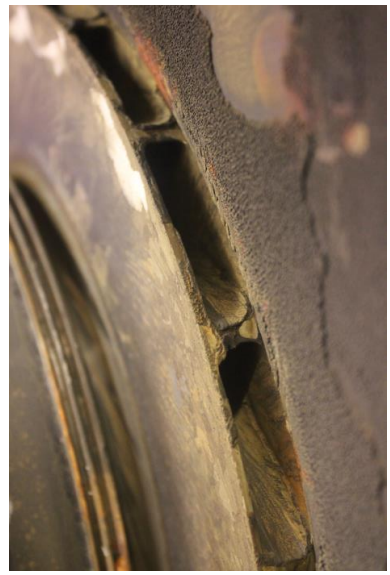

Figure 17 Wet gas compressor deliberately fouled during testing at K-Lab. The picture shows the impeller tip and the diffuser.

The fouling deposit depicted in Figure 17 was produced by injecting small amounts of water, ensuring theoretically complete evaporation inside the machine. The fouling thickness and surface roughness varied throughout the flow path of the machine and the sample thickness varied from 0.15 mm to 1.3 mm. As can be seen in Figure 17, the fouling is thick in some locations and thinner in others. This inhomogeneity was probably a result of the test programme, where fouling conditions were followed by heavy washing and this procedure was later repeated a second time before the compressor was dismantled.

Based on the fouling cases presented in Figure 16 to Figure 17, a representative deposit layer with a thickness of 1.4 mm and a roughness of approximately 500 µm was applied at the NTNU compressor impeller and diffuser section in areas as illustrated by Figure 18. An overview picture taken during the fouling application is given in Figure 19. The main contributions to increased losses will then be increased skin friction and increased blockage due to the thickness of the fouling layer.

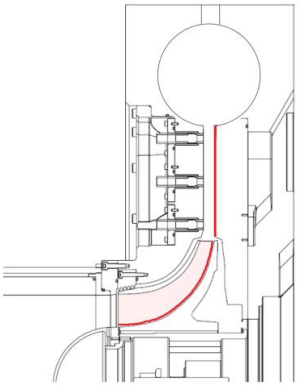

Figure 18 Cross-sectional drawing indicating where the deposit is applied. Dark red indicates deposit on the impeller hub and diffuser hub side. Light red indicates deposit on impeller vanes.

Figure 19 Picture taken during the application of fouling on the NTNU compressor. The picture was taken before shroud mounting.

The artificial 'fouling' deposits at the test lab compressor were made by applying a mixture of 'metal paint' blended with 'saw cutaway' of the material PMMA (poly(methyl methacrylate)). The fouling deposit was applied using a paint brush, and the deposit was applied in 11 layers to ensure a robust and uniform surface.

To analyse the test results, a UniSim model was built to represent the NTNU impeller test rig, see Figure 20. Furthermore, an ActiveX/COM interface was used between MATLAB and UniSim so that test data could be written and the results read from the UniSim model. The wet performance was estimated based on homogeneous wet fluid properties obtained from the UniSim model. The wet gas polytropic head and efficiency were calculated by equation Eq.(23), Eq.(25) and Eq.(26). The decreased discharge temperature in wet conditions leads to increased uncertainty in performance calculations that are based on enthalpies. Therefore, the torque meter power measurement was used as the power input for the compressor. The discharge temperature was thus calculated based on inlet conditions, discharge pressure and the torque meter power input.

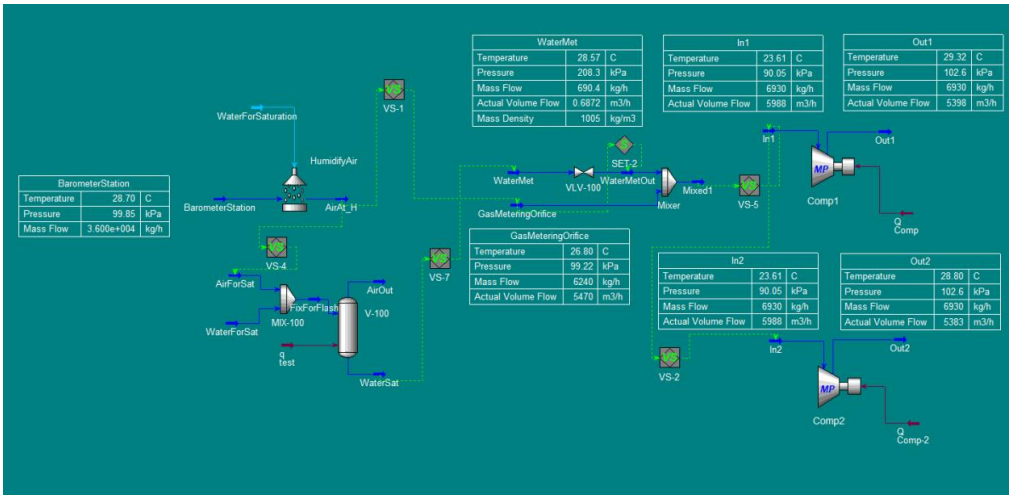

Figure 20 UniSim simulation case designed to calculate fouling results

4.4.1 Reynolds number correction

Geometric, kinematic and dynamic similarity are required for the comparison of results between conditions in model testing. In general, similar surface roughness between model and prototype is a similarity requirement [24], and a similar Reynolds number between conditions is one of the requirements for dynamic similarity [39]. However, in performance testing according to both ASME PTC 10 [2] and ISO 5389 [3], Reynolds number correction between the test and the specified condition is allowed. The correction is done according to the ICAAMC working group procedure [40]. This procedure provides a method for correcting efficiency, head coefficients and flow coefficient between the test and specified conditions. To evaluate the fouling effects on wet and dry performance, the ICAAMC procedure was chosen as the starting point. It was chosen because it is a well-established procedure for dry gas, and it would be interesting to see if adaptations for wet gas could be implemented. In the following, a derivation of the ICAAMC equation for efficiency correction is given.

Skin hydraulic losses can be compared to the losses in pipe flow, which are given by the Darcy-Weisbach equation

$$\frac{\Delta p_F}{L} = f\frac{\rho V^2}{2d} \tag{50}$$

Here, Δp_F is the pressure loss due to friction, L is the length, ρ is the density, V is the average velocity, d is the diameter and f is the Darcy friction factor. For the turbulent region, f can be found from the Colebrook equation [41]

$$\frac{1}{\sqrt{f}} = -2\log_{10}\left(\frac{2.51}{Re\sqrt{f}} + \frac{k_s}{3.7d}\right) \tag{51}$$

where Re is the Reynolds number. The roughness k_s is the equivalent sand roughness, representing a uniform grain size distribution that was used to produce the empirical data by Nikuradse [42]. For a machined surface, typically the arithmetic average roughness, R_a, is available. It is defined as

$$R_a = \frac{1}{n}\sum_{i=1}^{n}|y_i| \tag{52}$$

where y_i is the distance from the mean line of the i-th measurement. A method for relating the arithmetic average roughness R_a of a machined surface to the equivalent sand roughness is needed if Eq.(51)) is to be used. The method chosen by the ICAAMC working group [40] is $k_s/d = R_a/b_2$, where b_2 is the impeller tip width.

Here, the method motivated by Casey [43] for deriving the expression given by ICAAMC that relates loss between specified and test conditions is given. The efficiency of a compressor can be given as

$$\eta = \frac{\Delta \mathrm{h} - \Delta h_F - \Delta h_{f_{indep}}}{\Delta h} = 1 - f\frac{L}{d}\frac{V^2}{2\Delta h}\theta - \zeta \tag{53}$$

Here, Δh is the specific enthalpy increase over the machine, Δh_F the specific enthalpy loss caused by friction, $\Delta h_{f_{indep}}$ are the friction-independent specific enthalpy loss and ζ denotes the non-friction losses, assuming $V \propto u$, this expression can be simplified to

$$\eta = 1 - \frac{c}{\tau} f - \zeta \tag{54}$$

where τ is the work coefficient and c is a constant. The difference between two states of different friction factors, assuming ζ is constant, would then be

$$\eta_{sp} - \eta_t = \frac{c_t}{\tau_t} f_t - \frac{c_{sp}}{\tau_{sp}} f_{sp} \tag{55}$$

Further, assuming $c_{sp} = c_t$, and comparing dynamically similar conditions ($\tau_{sp} = \tau_t$), we can simplify further

$$\eta_{sp} - \eta_t = \frac{c}{\tau}(f_t - f_{sp}) \tag{56}$$

Casey [43] showed how Eq(54) could be used to derive the efficiency correction equation given in the ICAAMC paper [40] by defining the constant a as the fraction of losses at some limit of critical friction factor $a = \frac{\zeta}{\zeta + \frac{c}{\tau} f_{CR}}$:

$$\frac{\frac{1-\eta_{sp}}{1-\eta_{CR}}}{\frac{1-\eta_t}{1-\eta_{CR}}} = \frac{1-\eta_{sp}}{1-\eta_t} = \frac{a + (1-a)\frac{f_{sp}}{f_{CR}}}{a + (1-a)\frac{f_t}{f_{CR}}} \tag{57}$$

This is equal to the expression proposed by the ICAAMC working group, but they assign a the constant value of 0.3. One plausible reason why a apparently can be treated as a constant 0.3 as given by ICAAMC, is that most machines tested are close to hydraulically smooth and therefore will have similar limits for f_{CR}.

The main assumptions for this expression can be summarised as:

1. Friction losses can be calculated like losses in pipe flow.
2. The hydraulic diameter d in Eq.(53) is assumed constant between test and specified conditions.
3. Functions describing frictional losses are equal for all operational points $\theta = const$. This value is probably a function of operating condition $\theta(\phi)$ but can be treated as a constant when only evaluating performance change due to frictional factor change at the best efficiency point.
4. The kinematic and dynamic similarity between the test and specified conditions.
5. The non-friction losses are equal between the test and specified conditions $\zeta_{sp} = \zeta_t = \zeta$
6. The critical friction factor f_{CR} is equal in both the test and the specified conditions.

5 RESULTS AND DISCUSSION

This chapter summarizes the experimental results and theoretical analysis conducted as part of this thesis. First, it includes fundamental aspects relating to similarity and its limitation for wet gas compressor performance analysis. Secondly, the performance test result from a hydrocarbon centrifugal compressor test campaign is utilized to generate a novel method for modelling wet gas performance. Thirdly, it includes wet gas performance uncertainty analysis utilizing the Monte Carlo Method (MCM) and sensitivity analysis, and finally fouling test results are presented together with a proposed fouling correction method.

5.1 Similarity analysis for wet gas centrifugal compressor

The background and methods for this chapter are outlined in section 4.1. Based on the proposed definitions of the Machine Stokes number and the Machine Weber number given in section 4.1, some example values of these numbers are presented in Table 7. One case for Air/Water at atmospheric conditions and several cases for Rich gas/Condensate/water mixtures at actual conditions are tabulated. The inlet pressure, temperature, and droplet size are varied to obtain the listed values and the physical data for Rich gas/Condensate/water mixtures are based on typical equilibrium compositions as they would be in the K-lab VGII test loop.

Table 7 Example values of Machine Stokes numbers and Machine Weber numbers. Typical equilibrium composition values for Rich Gas/Condensate/Water mixtures for the VGII loop are presented.

Parameter	Air/water (NTNU)	RG/Cond ./water	RG/Cond ./water	RG/Cond ./water	RG/Cond ./water	RG/Cond ./water	RG/Cond ./water	RG/Cond ./water	RG/Cond ./water	RG/Cond ./water
P [bar]	1.0	46.5	100.0	100.0	20.0	20.0	100.0	100.0	20.0	20.0
T [°C]	20.0	13.5	20.0	60.0	20.0	60.0	20.0	60.0	20.0	60.0
$\sigma_{D_{water.drop}}$ [mN/m]	73.0	80.5	74.1	65.4	82.4	75.7	74.1	65.4	82.4	75.7
$\sigma_{D_{cond.drop}}$ [mN/m]	-	14.3	4.8	6.4	19.1	16.3	4.8	6.4	19.1	16.3
μ_G [Pa·s]	1.82E-05	1.20E-05	1.54E-05	1.55E-05	1.15E-05	1.26E-05	1.54E-05	1.55E-05	1.15E-05	1.26E-05
$d_D[\mu m]$	60.0	60.0	60.0	60.0	60.0	60.0	100.0	100.0	100.0	100.0
$\rho_{D_{cond.drop}}$ [kg/m^3]	-	729.0	631.9	672.3	757.2	731.7	631.9	672.3	757.2	731.7
$\rho_{D_{water.drop}}$ [kg/m^3]	998.0	999.3	998.0	983.8	997.6	982.6	998.0	983.8	997.6	982.6
ρ_G [kg/m^3]	1.2	40.5	109.3	87.8	16.3	16.1	109.3	87.8	16.3	16.1
U_2 [m/s]	150.0	150.0	150.0	150.0	150.0	150.0	150.0	150.0	150.0	150.0
b [m]	0.02	0.02	0.02	0.02	0.02	0.02	0.02	0.02	0.02	0.02
$Stm_{water\ drops}$ [-]	82.2	124.4	97.3	95.1	130.6	117.4	270.4	264.2	362.9	326.2
$Stm_{cond.\ drops}$ [-]	-	90.8	61.6	65.0	99.2	87.4	171.2	180.6	275.5	242.9
$Wem_{water\ drops}$ [-]	22	680	1989	1811	267	287	3315	3018	444	478
$Wem_{cond.\ drops}$ [-]	-	3833	30555	18482	1151	1333	50925	30803	1918	2221

The Machine Stokes number was higher for condensate droplets compared with water droplets due to higher droplet density for water. It is noteworthy that a similar Machine Stokes number can be targeted for atmospheric conditions (with water droplets) compared to hydrocarbon real conditions (with condensate droplets). However, for the Machine Weber number, this is not possible, as the number is substantially larger for real conditions compared to atmospheric conditions. This indicates that the breakup of droplets is more dominant in real conditions compared to atmospheric conditions, and more dominant for hydrocarbon droplets compared to water droplets.

5.1.1 Summary

- The problem of defining similarity conditions relating to wet compressor performance testing was exposed. Furthermore, the complexity of the wet gas compression process has been illuminated. Therefore, the need for test facilities where fundamental research can be carried out is of utmost importance.

- It has been shown by reasoning how the introduction of liquids into a compressor will complicate the flow field and that no general method for ensuring kinematic similarity between different operating conditions can be found. However, pragmatic approaches could give approximate solutions within certain limits.

- The problem of defining wet dynamic similarity parameters, such as the Machine Mach Number and Machine Reynolds number, was exposed and some suggestions for Machine Stokes and Weber number were proposed.

- The issue of how to define a Type2 test for wet gas compressor performance has been exposed. It is still not clear if Type2 testing of wet gas compressors is possible, i.e., it is not clear whether kinematic and dynamic similarity can be adequately fulfilled to allow for the comparison of results between the test and specified conditions (when the test and specified conditions deviate significantly).

5.2 Creating a model for the wet gas hydrocarbon centrifugal compressor test results

The background and methods for this chapter are outlined in section 4.2. The test matrix for the performance mapping that was conducted is given in Table 8. Every row in this table is a set of curves, which have the same speed, suction pressure, suction temperature, and the same type of liquid injected. The *GMF* range for every curve set is given in the table, and every curve in the curve set contains 5 (6 for some cures to investigate boundaries) points taken at different flow rates ranging between surge and choke. The curve set name convention is indicated by relative pressure-relative speed-liquid type, where relative refers to the design values. The selected test matrix for performance mapping gives a representative range of test points both at design and off design conditions. Furthermore, it spans typical liquid loads for gas/condensate well streams.

Table 8 The test matrix for the two-impeller centrifugal compressor tested at K-Lab. Suction pressure and compressor speed are given as percentages of the design values. *Water and hydrocarbon liquid were injected in equal mass amounts.

Curve set Name	p_1 % bar design	Speed % rpm design	*GMF*	Liquid type	Dr $\frac{\rho_l}{\rho_g}$	Visc Ratio $\frac{\mu_l}{\mu_g}$
100-100-HC	100	100	[1.0 0.95 0.9 0.8 0.7]	HC	15	40
100-90-HC	100	90	[1.0 0.95 0.9 0.8 0.7]	HC	15	40
100-90-HC+Aq	100	90	[1.0 0.95 0.9 0.8 0.7]	HC+Aq*	18	44
125-90-HC	125	90	[1.0 0.95 0.9 0.8]	HC	12	39
55-90-HC	55	90	[1.0 0.95 0.9 0.8 0.7]	HC	30	58
100-80-HC	100	80	[1.0 0.95 0.9 0.8 0.7]	HC	15	40

Figure 21 shows the resulting pressure ratio vs normalized flow coefficient curves for all curve sets taken at 90% of the design speed with pure hydrocarbon liquid as the injected liquid. Notice how the crossing point for when liquid injection gives increased pressure ratio shifts towards the right as the suction pressure increases (i.e., when the density ratio $\frac{\rho_l}{\rho_g}$ decreases).

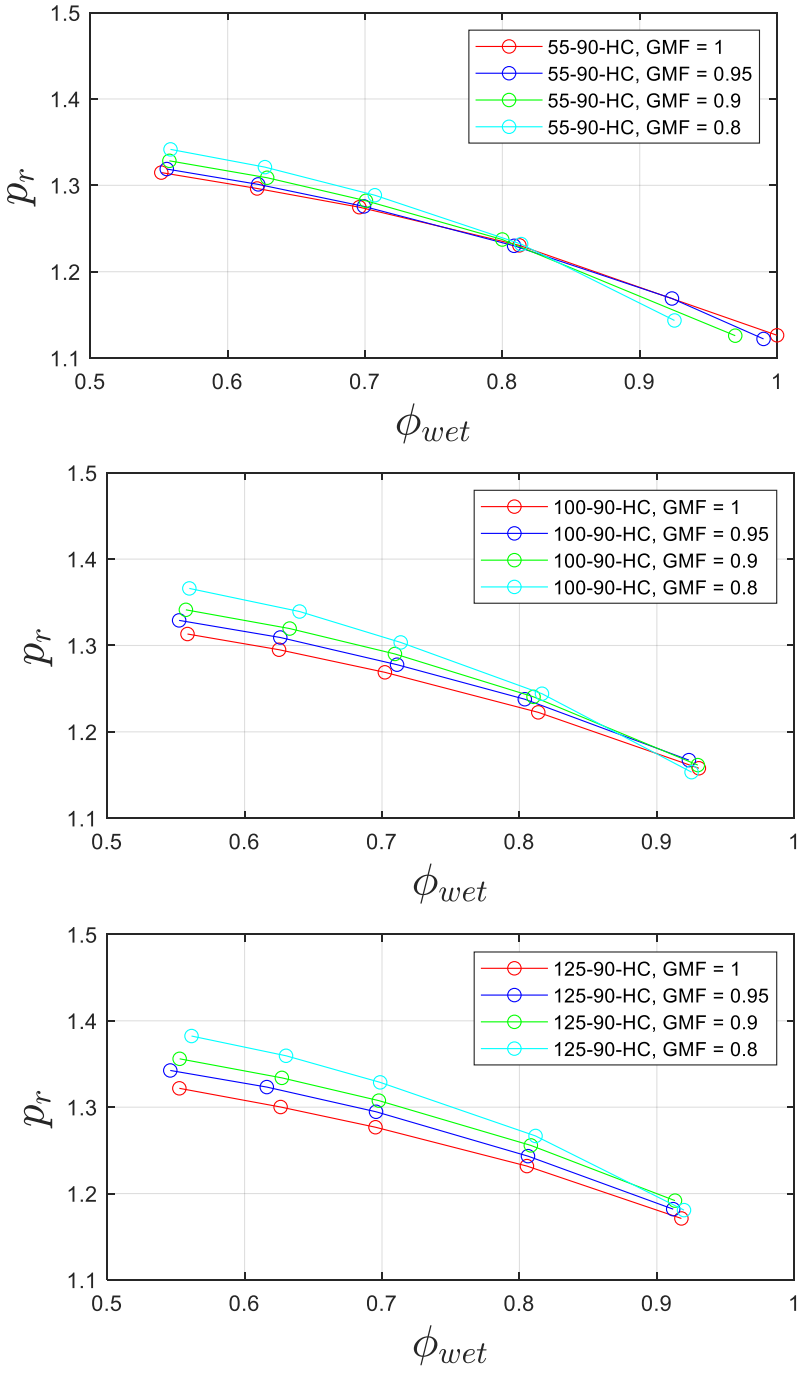

Figure 21 The pressure ratio vs normalized flow coefficient. The curve set name convention is indicated by: percent of design pressure – percent of design speed – liquid type.

To model the change in wet performance for different operating conditions, several variants of the wet variable Γ were tested to investigate which dimensionless variables were suited for modelling wet performance. All variables were defined at inlet conditions. An example of a simple variant of Γ, that gave good model prediction is given by

$$\Gamma(GMF, GVF) = GMF^{a_1} GVF^{a_2} \tag{58}$$

This variant is indirectly linked to densities, as shown in Eq.(6) because the ratio of *GVF* to *GMF* equals the ratio of mix density to gas density for homogeneous flow.

As the density ratio relates to the separation of phases and the viscosity ratio relates to the pressure loss and entropy generation in the flow, we assert that these variables are related to both the wet- polytropic head coefficient and efficiency. Inspired by the original work by Lockhart and Martinelli[13] for estimation of pressure loss in two-phase flow, a similar variant for Γ was tested. This variant is given by

$$\Gamma\left(\frac{\dot{m}_l}{\dot{m}_g}, \frac{\rho_g}{\rho_l}, \frac{\mu_l}{\mu_g}\right) = \left(\frac{\dot{m}_l}{\dot{m}_g}\right)^{a_1} \left(\frac{\rho_g}{\rho_l}\right)^{a_2} \left(\frac{\mu_l}{\mu_g}\right)^{a_3} \tag{59}$$

and defined as zero when $\dot{m}_l = 0$. This variant provides a very good model for both the polytropic head coefficient and polytropic efficiency. Figure 22 illustrates the modelled normalized polytropic head coefficient as a function of the normalized flow coefficient and the wet variable defined by Eq.(59). Here the model is represented by the surface, plotted together with the data points for all the curve sets. The model gives a good representation of the tested data. One advantage of the proposed method is that it allows for visualization of the model in 3D plots.

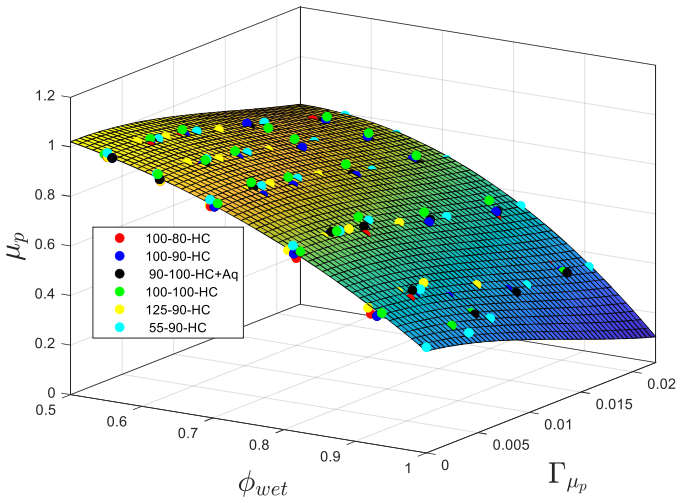

Figure 22 Normalized polytropic head coefficient plotted against normalized flow coefficient and the wet variable Γ. The model is the surface shown in the plot.

Figure 23 shows modelled vs measured normalized polytropic head coefficient for all test points. The model captures the variation in polytropic head to a large degree. Figure 24 shows a residual plot for the normalized polytropic head coefficient. For these normalized data, the predicted values show error within ±0.04, while most errors are within ±0.02

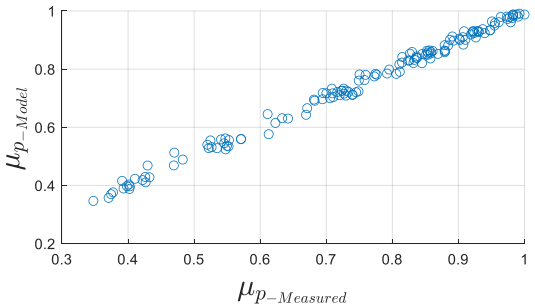

Figure 23 Plot showing model vs test data for normalized polytropic head coefficient.

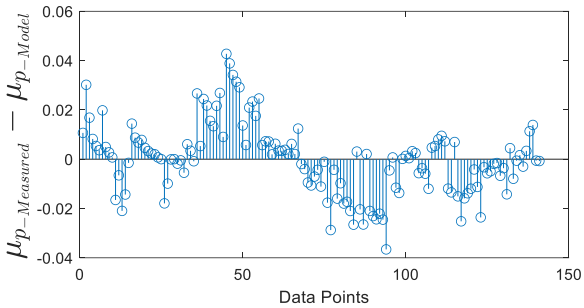

Figure 24 Residual plot for normalized polytropic head coefficient.

Figure 25 illustrates the modelled normalized polytropic efficiency as a function of the normalized flow coefficient and the wet variable defined by Eq.(59). The model is represented by the surface, plotted together with the data points for all the curve sets. Also, for polytropic efficiency, the model gives a good representation of the tested data.

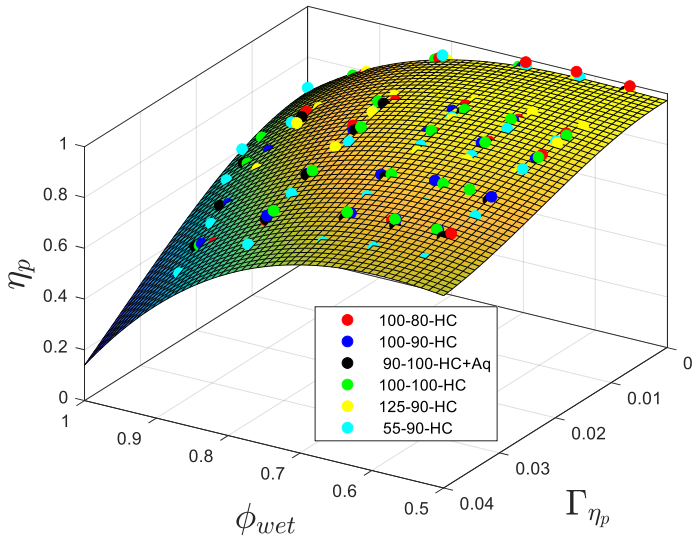

Figure 25 Normalized polytropic efficiency plotted against normalized flow coefficient and the wet variable Γ. The model is the surface shown in the plot.

Figure 26 shows modelled vs measured polytropic efficiency coefficient for all test points. The model also captures the variation in polytropic efficiency to a large degree. Figure 27 shows a residual plot for normalized polytropic efficiency. For these normalized data, all predicted values show errors within ±0.04, while most errors are within ±0.02.

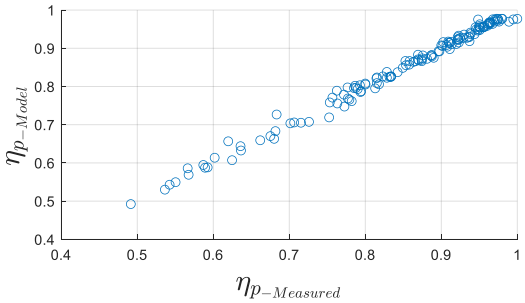

Figure 26 Plot showing model vs test data for normalized polytropic efficiency.

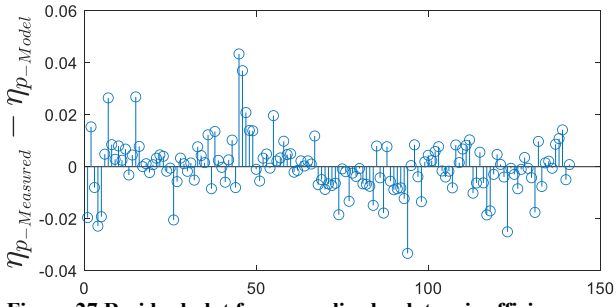

Figure 27 Residual plot for normalized polytropic efficiency.

Many combinations of inputs to the wet variable Γ can be chosen, and it is interesting to investigate the resulting goodness of different choices. Goodness of fit parameters for a selection of Γ variants is summarized in Table 9 and Table 10**.**

Table 9 Regression result for the Polytropic Head coefficient for different variants of the wet variable Γ_{μ_p}.

Predicted variable	Wet variable Γ_{μ_p}	SSE	R^2	R^2-adj	RMSE
μ_p	GVF^{a_1}	0.1398	0.970	0.968	0.0327
μ_p	GMF^{a_1}	0.0406	0.991	0.991	0.0176
μ_p	$\left(\frac{\rho_m}{\rho_g}\right)^{a_1}$	0.0368	0.992	0.992	0.0168
μ_p	$\left(\frac{a_m}{a_g}\right)^{a_1}$	0.0334	0.993	0.992	0.0160
μ_p	$GMF^{a_1}GVF^{a_2}$	0.0298	0.994	0.993	0.0151
μ_p	$\left(\frac{\dot{m}_l}{\dot{m}_g}\right)^{a_1}\left(\frac{\rho_g}{\rho_l}\right)^{a_2}\left(\frac{\mu_l}{\mu_g}\right)^{a_3}$	0.0290	0.994	0.993	0.0149
μ_p	$GMF^{a_1}Ma_{wet}^{a_2}$	0.0246	0.995	0.994	0.0137
μ_p	$Ma_{wet}^{a_1}\left(\frac{\rho_m}{\rho_g}\right)^{a_2}$	0.0204	0.996	0.995	0.0125
μ_p	$Ma_{wet}^{a_1}\left(\frac{\rho_g}{\rho_m}\right)^{a_2}\left(\frac{\mu_m}{\mu_g}\right)^{a_3}$	0.0127	0.997	0.997	0.0098

Table 10 Regression result for Polytropic efficiency for different variants of the wet variable Γ_{η_p}.

Predicted variable	Wet variable Γ_{η_p}	SSE	R^2	R^2-adj	RMSE
η_p	GVF^{a_1}	0.1896	0.906	0.899	0.0380
η_p	GMF^{a_1}	0.0445	0.978	0.976	0.0184
η_p	$GMF^{a_1}Ma_{wet}^{a_2}$	0.0431	0.979	0.977	0.0181
η_p	$\left(\frac{\rho_m}{\rho_g}\right)^{a_1}$	0.0380	0.981	0.980	0.0170
η_p	$Ma_{wet}^{a_1}\left(\frac{\rho_m}{\rho_g}\right)^{a_2}$	0.0363	0.982	0.981	0.0167
η_p	$\left(\frac{a_m}{a_g}\right)^{a_1}$	0.0316	0.984	0.983	0.0155
η_p	$GMF^{a_1}GVF^{a_2}$	0.0176	0.991	0.991	0.0116
η_p	$\left(\frac{\dot{m}_l}{\dot{m}_g}\right)^{a_1}\left(\frac{\rho_g}{\rho_l}\right)^{a_2}\left(\frac{\mu_l}{\mu_g}\right)^{a_3}$	0.0159	0.992	0.992	0.0110
η_p	$LMF^{a_1}\left(\frac{\mu_l}{\mu_g}\right)^{a_2}\left(\frac{\rho_g}{\rho_l}\right)^{a_3}$	0.0149	0.993	0.992	0.0107
η_p	$LMF^{a_1}LVF^{a_2}\left(\frac{\mu_l}{\mu_g}\right)^{a_3}$	0.0143	0.993	0.992	0.0104

Indeed, several variants give good models for the test data set at hand. Furthermore, it is interesting to notice that simple variants that rely only on *GMF* and *GVF* or of *GVF* and density ratio give quite representative models. However, the best models are given by including viscosities, the velocity of sound, and the wet Mach number.

5.2.1 Measurement and model uncertainties

The instrumentation used to retrieve the analysed data was in accordance with the ASME PTC 10 performance test code and includes flow orifice, pressure- and temperature metering at suction and discharge, and torque meter for power measurements. Typical values for relative standard uncertainty of performance parameters are summarized in Table 11.

Table 11 Typical values for relative standard uncertainty of performance parameters

Variable	Dry $u(k=2)$ [%]	Wet $u(k=2)$ [%]
μ_p	0.7	1.0
η_p	1.7	2.0
ϕ	1.0	1.0

It is important to be aware that overfitting is a potential issue when building models and should be addressed to avoid failure when applying the model for prediction on future observations. By reducing the number of input parameters inserted into the wet variable Γ, given by Eq.(47), the degrees of freedom are reduced, thus the risk of overfitting is lowered. Another way of reducing the degrees of freedom could be to utilize a second-order polynomial instead of a third-order polynomial for the modelled surface given by Eq.(45) and Eq.(46). Furthermore, methods for reducing the risk of overfitting, such as the K-fold cross-validation, should be implemented in the future development of the proposed method for the wet gas performance model.

5.2.2 Summary

- Test results obtained from a two-impeller centrifugal compressor tested at K-Lab at varying operating conditions have been analysed. Based on these data a new method for generating a wet gas compressor performance model has been proposed. This model merges identified key dimensionless parameters into a new wet variable.

- Identified key parameters affecting wet performance are *GVF*, *LVF*, or density ratio of liquid to gas. However, when including viscosity and wet Mach number, the model describes the performance variation to the greatest extent.

- The proposed model can predict both the polytropic head coefficient and polytropic efficiency according to the available test data. The proposed method is generic in the sense that it can easily be tuned for other machines and expanded to include other variables. Another advantage of the proposed method is that it merges all identified variables into one wet variable, thus a 3D plot representing the wet performance can easily be generated.

- The presented results indicate that wet performance curves can be generated for centrifugal compressors. To establish such curves, some wet performance mapping will be necessary. Mapping of varying *GMF*'s and at a representative range of density ratios to allow for a model that can be utilized for an appropriate range of operating conditions is recommended. To further develop the model, mapping with fluids of varying viscosity will also be an advantage

5.3 Uncertainty and sensitivity analysis for wet gas compressor test results

The background and methods for this chapter are outlined in section 4.3. Figure 28 and Figure 29, show resulting Monte Carlo simulations for the operating point of the wet cases. Here, the operating points for mechanically determined polytropic efficiency $\boldsymbol{\eta_{pM}}$ and thermodynamically determined polytropic efficiency $\boldsymbol{\eta_{pT}}$ versus flow are depicted. All wet cases given in Table 6 are given in these plots. It is clear that the choice of EOS affects both the mechanically determined and thermodynamically determined efficiency and that the polar components model only affects the thermodynamically determined polytropic efficiency. It is noteworthy to see how great the uncertainty is in the thermodynamically determined polytropic efficiency, compared to the mechanically determined polytropic efficiency. This significant difference arises from the specific enthalpy uncertainty that is significantly greater when determined from the thermodynamics compared to torque meter and mass flow. Furthermore, the mechanically determined enthalpy change is not affected by the polar components model, while the thermodynamically determined enthalpy change shows a strong dependence on both the EOS and polar components model.

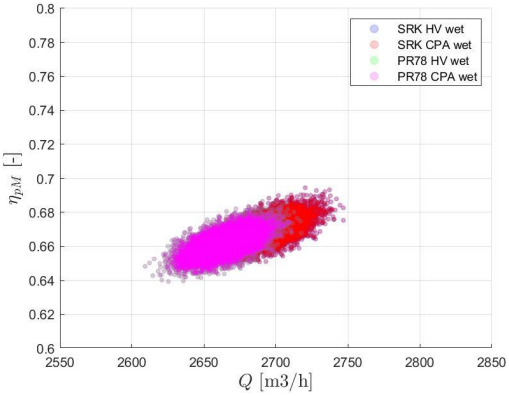

Figure 28 Operating point wet case, given by the polytropic mechanically determined efficiency versus actual flow

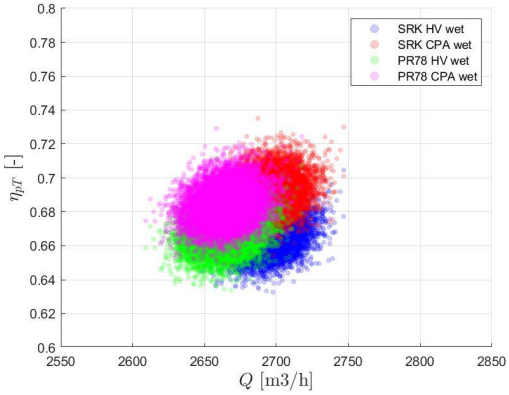

Figure 29 Operating point wet case, given by the thermodynamically determined polytropic efficiency versus actual flow

The resulting uncertainty data for compressor performance parameters are presented in Table 12 and Table 13.

Table 12 MCM uncertainty for the PR78 HV wet case

Measurand	$\bar{y}$	$u\ (k=1)$	$\frac{u}{\bar{y}} * 100\%$	95% Coverage interval
h_p[kJ/kg]	23.51	0.12	0.52	[23.27-23.75]
P_T [kW]	1524	21	1.4	[1483-1566]
P_M [kW]	1540	10	0.65	[1521-1560]
η_{pT} [-]	0.669	0.010	1.5	[0.650-0.689]
η_{pM}[-]	0.6618	0.0064	0.97	[0.6492-0.6745]
Q [m^3/h]	2665	14	0.54	[2636-2693]
LMF [-]	0.1384	0.0011	0.79	[0.1363-0.1405]
GVF [-]	0.98990	0.00010	0.010	[0.98970-0.99009]

Table 13 MCM uncertainty for the PR78 HV Dry Case

Measurand	$\bar{y}$	$u\ (k=1)$	$\frac{u}{\bar{y}} * 100\%$	95% Coverage interval
h_p[kJ/kg]	37.77	0.13	0.36	[37.51-38.04]
P_T [kW]	1685	16	0.97	[1653-1717]
P_M [kW]	1700	10	0.59	[1681-1720]
η_{pT} [-]	0.8372	0.0080	0.95	[0.8219-0.8532]
η_{pM}[-]	0.8299	0.0072	0.86	[0.8158-0.8441]
Q [m^3/h]	2638	14	0.54	[2610-2666]

Here, the average output parameter value, together with the standard uncertainty (k=1), relative standard uncertainty in percent, and the 95% coverage interval is given. As can be seen from these results, compressor performance parameters that strongly depend on thermodynamic enthalpies have significantly greater uncertainty for the wet case compared to the dry case. This can be seen in the standard uncertainties of the thermodynamically determined power and efficiency. Furthermore, the expected uncertainties are greater for wet compared with dry performance parameters. When liquid is injected into a compressor, the discharge temperature is significantly reduced. The lowering of the temperature difference over the machine will make the uncertainties more sensitive to temperature for the wet case compared to the dry case. Furthermore, if additional uncertainties would be assigned to multiphase temperature measurements, this effect will be even greater. One example of increased multiphase temperature uncertainty could be if equilibrium is not reached at compressor discharge, then the gas and liquid temperature could be different, and the measured temperature would no longer represent the equilibrium temperature. The significant reduction in uncertainties for compressor performance parameters that rely on a directly measured power, as compared with thermodynamically determined power, is thus clear.

Since characterization cannot be performed programmatically in PVTsim, the effect of random variation of the C6-C10+ molecular weights and densities on characterization could not be investigated. Therefore, any impact in phase split and flash properties arising from "random characterization", which ultimately will have some effect on compressor performance, could not be assessed.

5.3.1 Sensitivity analysis for a wet gas compressor system

Figure 30 provides a typical example of the scatter plot analysis. Here, it is clear that the variation in the polytropic head is highly correlated with inlet pressure and has a low correlation with inlet temperature. The analysis of scatter plots is also an efficient way to look for nonlinearities, which can be identified as bent scatter plots. The scatter plots for all compressor performance parameters versus all input parameters were investigated by visual inspection and no significant nonlinearities were found.

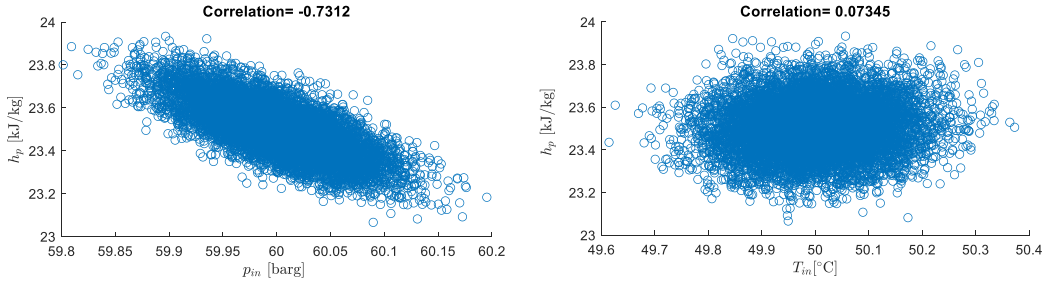

Figure 30 Scatter plot for the Polytropic head versus inlet pressure and inlet Temperature

As the sigma-normalized derivatives, $\boldsymbol{\theta}^{\boldsymbol{\sigma}}_{\boldsymbol{x_i}}$, are very similar for all combinations of PVTsim settings listed in Table 6, the resulting, $\boldsymbol{\theta}^{\boldsymbol{\sigma}}_{\boldsymbol{x_i}}$, are only presented for PR78 EOS with the HV polar components model for the wet and dry case. The top 10 sensitivities for selected performance parameters are given in Table 14 and Table 15 for the wet and dry case, respectively. The uncertainties are dominated by pressure and temperature at the inlet and discharge, for the wet case, some effects from the composition uncertainties are seen especially from the C10+ in the oil loading. Furthermore, the torque power dominates the uncertainties for mechanically determined efficiency. These results show the importance of having good control over pressure and temperature measurements at the compressor inlet and discharge. Temperature is especially important for parameters that rely on thermodynamic enthalpy calculations, while mechanically determined parameters rely strongly on torque meter uncertainty, as well as uncertainties relating to flow, such as gas orifice pressure and differential pressure. The sensitivities relating to inlet and outlet pressure and temperature are not surprising, as the requirements in ASME PTC10 [2] are four pressure and four temperature sensors on both inlet and discharge of the compressor during performance testing.

Table 14 Top 10 sigma-normalized derivatives for selected performance parameters for the wet PR78 HV case

h_p		η_{P_T}		η_{P_M}		P_T	
x_i	$\theta^{\sigma}_{x_i}$	x_i	$\theta^{\sigma}_{x_i}$	x_i	$\theta^{\sigma}_{x_i}$	x_i	$\theta^{\sigma}_{x_i}$
p_{in}	-0.73	T_{in}	0.60	P_M	-0.67	T_{out}	0.66
p_{out}	0.57	T_{out}	-0.59	p_{in}	-0.39	T_{in}	-0.63
$X_{Oil\ C10+}$	0.22	p_{in}	-0.35	p_{out}	0.31	$X_{Oil\ C10+}$	-0.19
$\dot{m}_{Aq\ Cori}$	-0.12	p_{out}	0.28	$p_{orifice}$	0.09	p_{in}	0.10
$\dot{m}_{Oil\ Cori}$	-0.12	$X_{Oil\ C10+}$	0.22	$\Delta p_{orifice}$	0.07	$\dot{m}_{Aq\ Cori}$	0.10
T_{Sep}	-0.12	$\dot{m}_{Aq\ Cori}$	-0.09	$X_{Oil\ C10+}$	0.06	p_{out}	-0.09
$X_{Gas\ C1}$	0.09	$\dot{m}_{Oil\ Cori}$	-0.07	$T_{orifice}$	-0.05	$\dot{m}_{Oil\ Cori}$	0.08
$X_{Oil\ nC4}$	-0.07	T_{Sep}	-0.06	T_{Sep}	-0.03	$p_{orifice}$	0.05
$X_{Gas\ C2}$	-0.07	$X_{Oil\ nC4}$	-0.02	$X_{Gas\ C1}$	0.03	T_{Sep}	0.04
m_{Gas}	-0.06	$X_{Oil\ nC5}$	-0.02	T_{out}	0.02	$\Delta p_{orifice}$	0.04
	.		.		.		.
	.		.		.		.
	.		.		.		.
$\sum_{i=1}^{k}(\theta^{\sigma}_{x_i})^2$	1.00		0.98		0.73		0.92

Table 15 Top 10 sigma-normalized derivatives for selected performance parameters for the dry PR78 HV case

h_p		η_{P_T}		η_{P_M}		P_T	
x_i	$\theta^{\sigma}_{x_i}$	x_i	$\theta^{\sigma}_{x_i}$	x_i	$\theta^{\sigma}_{x_i}$	x_i	$\theta^{\sigma}_{x_i}$
p_{in}	-0.78	T_{in}	0.61	P_M	-0.68	T_{out}	0.60
p_{out}	0.56	T_{out}	-0.59	p_{in}	-0.32	T_{in}	-0.57
$X_{Gas\ C1}$	0.27	p_{in}	-0.42	p_{out}	0.23	p_{in}	0.12
$X_{Gas\ C3}$	-0.17	p_{out}	0.31	$p_{orifice}$	0.11	p_{out}	-0.10
$X_{Gas\ C2}$	-0.13	$X_{Gas\ C1}$	0.05	$\Delta p_{orifice}$	0.08	$p_{orifice}$	0.09
$X_{Gas\ nC4}$	-0.10	$X_{Gas\ C3}$	-0.04	$T_{orifice}$	-0.06	$\Delta p_{orifice}$	0.07
$X_{Gas\ CO2}$	-0.09	$X_{Gas\ C2}$	-0.02	$X_{Gas\ C1}$	0.06	$T_{orifice}$	-0.05
T_{in}	0.07	$X_{Gas\ nC4}$	-0.02	$X_{Gas\ C3}$	-0.03	$X_{Gas\ CO2}$	-0.02
$X_{Gas\ iC4}$	-0.06	$X_{Gas\ iC4}$	-0.02	T_{in}	0.03	$X_{Gas\ C3}$	0.01
T_{out}	0.06	$X_{Gas\ nC5}$	-0.01	$X_{Gas\ C2}$	-0.03	$X_{Gas\ nC4}$	0.01
	.		.		.		.
	.		.		.		.
	.		.		.		.
$\sum_{i=1}^{k}(\theta^{\sigma}_{x_i})^2$	1.07		1.00		0.65		0.72

Figure 31, Figure 32 and Figure 33 show the sigma-normalized derivatives for all input variables for the polytropic head and mechanically and thermodynamically determined polytropic efficiency. This type of plot gives an excellent overview of the dominant sensitivities of input parameters.

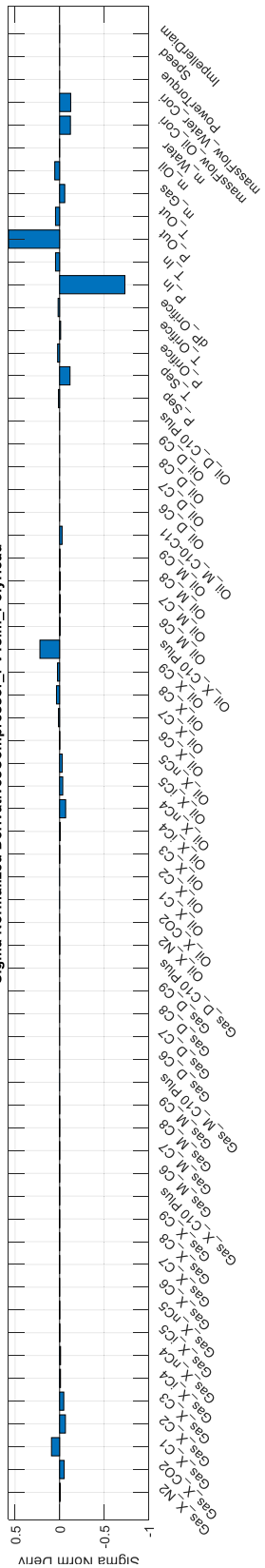

Figure 31 Sigma normalized derivatives polytropic head

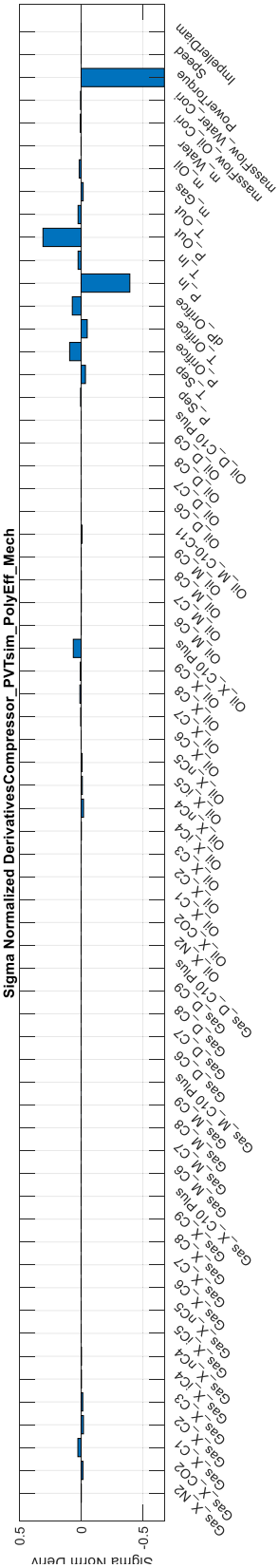

Figure 32 Sigma normalized derivatives for the mechanically determined polytropic efficiency

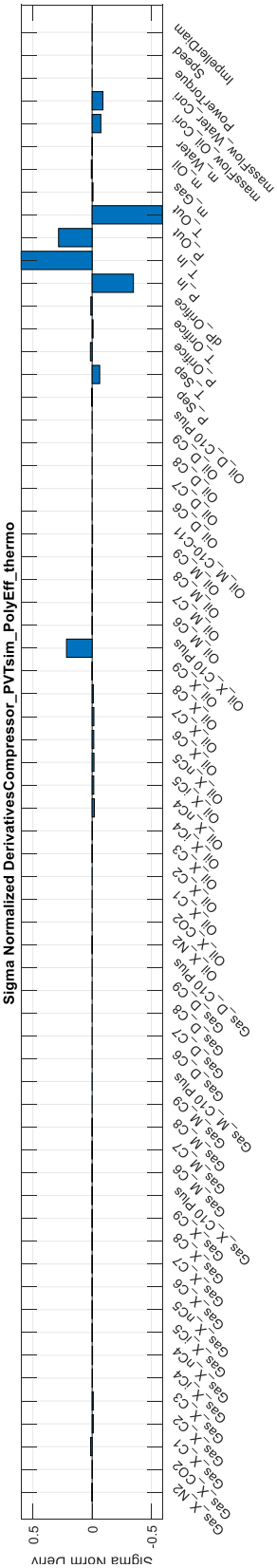

Figure 33 Sigma normalized derivatives for the thermodynamically determined polytropic efficiency

5.3.2 Additional considerations

Water content in the oil phase often referred to as water cut, is a quantity that is always present in a multiphase test loop. The water cut will vary based on the efficiency of the separation system, oil type, pressure and temperature. For simplicity, no value for water cut, or its associated uncertainty has been included in the selected cases. As the wet case investigated included injection of both oil and water, any extra uncertainty will typically be very limited. However, in a pure oil injection test point, any water cut will have a substantial effect on thermodynamic calculations due to the large enthalpy of vaporization for the water as compared to oil. Therefore, any water cut not accounted for will lead to a large bias in the calculations.

Gas density is necessary for orifice calculations and compressor performance calculations. Uncertainties relating to gas density have several sources: The main separator flash gives a gas composition that varies based on which EOS was used for the main separator flash. This will result in a different gas density based on which EOS has been chosen. Furthermore, different EOS gives different gas densities for identical compositions. This effect varies with pressure temperature and composition, and no general statement can be made. The GERG equation of state has been shown to give very low uncertainty for density, ±0.1% (k = 2), given input parameters within the validity range of temperature, pressure and compositions [44]. The GERG equation is limited to 21 available components. Examples of differences in gas density and mass flow between different EOS are given in Table 16. Here, $\rho_{orifice}$ and $\dot{m}_{orifice}$ is the gas density and mass flow calculated with the same EOS and polar components model as the main separator flash. Calculations of $\rho_{orificeGerg}$ and $\dot{m}_{orificeGerg}$, have been used by applying the resulting compositions for the listed choices of EOS and polar components models, and the C6-C10+ pseudo components have been assigned to associated normal alkanes nC6-nC10, which are available for GERG.

Table 16 Comparison of gas density and mass flows resulting directly from the selected EOS and gas using GERG on the orifice conditions (composition, pressure, and temperature)

	PR78 CPA	PR78 HV	SRK CPA	SRK HV
$\rho_{orifice}$ [kg/m^3]	50.98	50.98	49.87	49.87
$\rho_{orificeGerg}$ [kg/m^3]	50.20	50.20	50.13	50.12
$\dot{m}_{orifice}$ [kg/s]	37.36	37.36	36.95	36.95
$\dot{m}_{orificeGerg}$ [kg/s]	37.07	37.07	37.04	37.04

The differences in gas density and mass flows for the different EOS are obvious and it is important to note that these can be much greater for other pressures, temperatures and gas compositions [45]. Hence it is recommended to use dedicated instruments for measurement of gas density to assure reliable quality of gas density and mass flow estimates.

5.3.3 Summary

Uncertainties for wet gas performance parameters resulting from a wet gas test loop have been investigated. For comparison, a dry gas case was included. The uncertainties were propagated using the MCM, and a sensitivity analysis was conducted. The main results are:

- Compared to dry gas, significantly greater uncertainties were found for wet gas test results that rely on thermodynamically determined enthalpies.
- Many of the performance parameters are highly sensitive to inlet and discharge temperature, especially those relying on enthalpies.
- Additional uncertainties are expected for wet gas temperature measurements, as fluid thermal equilibrium may not be fulfilled. It is therefore strongly recommended to include additional power measurements in wet gas testing, e.g., torque meter or motor power measurements.
- For wet gas performance parameters that rely on enthalpies, the choice of polar components model is as important as the choice of EOS.

- As PVTsim Nova 4 cannot characterize programmatically, propagation of uncertainties through the characterization was not possible. Thus, it is recommended that this effect be further investigated.
- The correlation resulting from the normalization of compositional data was exposed. This problem arises both for the MCM and for step-change in the sensitivity analysis. This problem has not previously been exposed in the context of wet gas compressor testing. Two approaches for sampling random compositional data were proposed, one for gas and one for condensate.
- The benefits of direct gas density measurement have been exposed.

5.4 Fouling effects on wet gas centrifugal compressor performance

The background and methods for this chapter are outlined in section 4.4. A test matrix was chosen to investigate the effect of fouling in wet conditions compared to dry conditions. To avoid substantial damage to the fouling layer, some limitations had to be implemented to the test matrix. Consequently, only one speed line was chosen for the test campaign and only five points were run per *GMF* for the fouled conditions compared with six points for the clean condition. The test matrix is listed in Table 17.

Table 17 Test matrix

Parameter	Data
Speed	9000 rpm
GMF	1/0.98/0.95/0.9
Flow	Surge to choke
Condition	Clean/fouled

The resulting polytropic efficiency versus inlet flow coefficient curves for the whole test matrix is given in Figure 34, where the data points are given together with a second-order polynomial fit for all curves.

The general trend of decreasing efficiency for increasing liquid content, as well as the highly negative effect of fouling on efficiency are evident. The strong effect of friction losses caused by fouling can be seen from the divergence of clean and fouled curves of the same *GMF* as the flow is increased. It is interesting to note how all the clean curves have similar shapes, and how all fouled curves have similar shapes with a steeper characteristic in the high flow region.

The polytropic head versus inlet flow coefficient is given in Figure 35. The decrease in the head for the fouled machine, as well as the effect of decreasing head for increasing liquid injection, are seen in this plot. The same general trends as for the efficiency curves are observed for the polytropic head.

The work coefficient versus inlet flow coefficient is given in Figure 36. The work coefficient is very similar for all curves except *GMF*=0.90 which display a significantly greater work coefficient. Changes in the work coefficient can be assigned to changes in the impeller discharge velocity triangles.

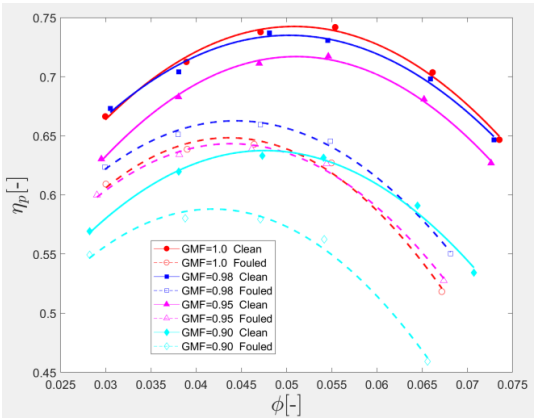

Figure 34 Polytropic efficiency versus inlet flow coefficient.

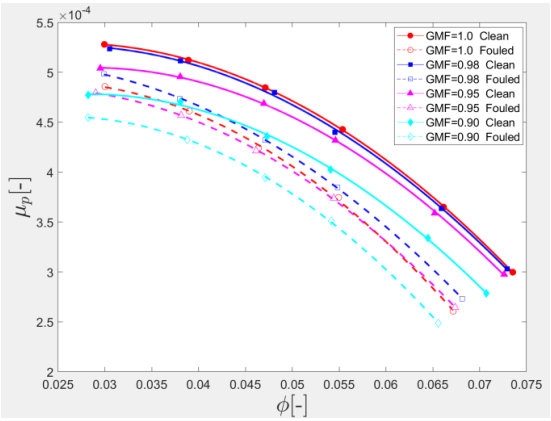

Figure 35 Polytropic head coefficient versus inlet flow coefficient.

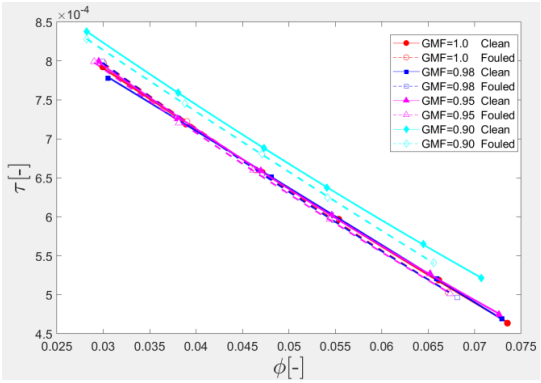

Figure 36 Work coefficient versus inlet flow coefficient.

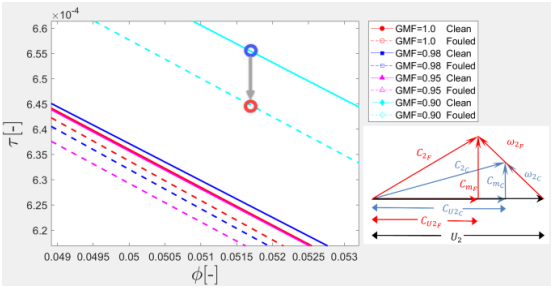

Figure 37 Close-up of work coefficient versus inlet flow coefficient, in the area of best efficiency. This plot makes the shift between clean and fouled curves for the same *GMF* visible. The illustration on the right shows an example of impeller discharge velocity triangles for a clean and fouled compressor.

Changes in the work coefficient can be assigned to changes in the impeller discharge velocity triangles. Several factors affect the shift in work coefficient. Figure 37. shows a close-up in the area around the best efficiency point. Here, one notices that the work coefficient for all fouled curves lies below the clean curves for the same *GMF*. This suggests that the effect of increased area blockage for the fouled impeller, combined with the effect of increased evaporation caused by increased friction losses dominates this region of the curve. Both effects lead to increased meridional velocity at the impeller tip, thus altering the impeller discharge velocity triangles as illustrated in Figure 37.

5.4.1 Proposed model for the impact of liquid and fouling on compressor performance

An attempt was made to create a model for correcting all efficiency curves to the dry clean curve. All calculations were based on the second-order polynomial fits of the measured data.

By assuming the clean surface roughness to be $R_a = 2\ \mu$m, an effective surface roughness (apparent roughness for the compressor as a whole) for the fouled machine was estimated to $R_a = 31\ \mu$m.

In the ICAAMC procedure, efficiency, polytropic work coefficient, work coefficient and flow coefficient are corrected between test and specified conditions. The correction in flow coefficient is given by

$$\frac{\phi_{sp}}{\phi_t} = \sqrt{\frac{\mu_{sp}}{\mu_t}} \tag{60}$$

where $\mu_{sp} = \frac{h_{p_{sp}}}{u_{sp}^2}$ and $\mu_t = \frac{h_{p_t}}{u_t^2}$ is the polytropic head coefficient under specified and test conditions, respectively. To allow for a flow coefficient shift that better corresponds with the measured data, the following correction was used for efficiency

$$\frac{\eta_{sp}}{\eta_t}\frac{1}{GMF} = 1.029\frac{\phi_{sp}}{\phi_t} \tag{61}$$

The best efficiency points found for all second-order polynomial fits were used to generate the regression coefficient of 1.029. Here, the specified condition sp was taken to be the clean and dry condition and the test condition t all the other conditions. This correction is based on a limited data set and thus subject to some uncertainty. However, it will serve as a first attempt.

First, the dry case was considered. The proposed model for the difference in loss between two conditions given by Eq.(56) was applied

$$\eta_{clean} - \eta_{fouled} = \frac{c}{\tau_{fouled}}(f_{fouled} - f_{clean}) \tag{62}$$

Eq(61) and Eq.(62) was used to correct efficiency and flow coefficient, respectively at the best efficiency point. The whole curve was corrected using the same values for efficiency correction and flow coefficient correction found at the best efficiency point. The constant c was tuned to get the best fit for the correction between clean and fouled condition for the entire curve. The resulting corrected curves are given in

Figure 38.

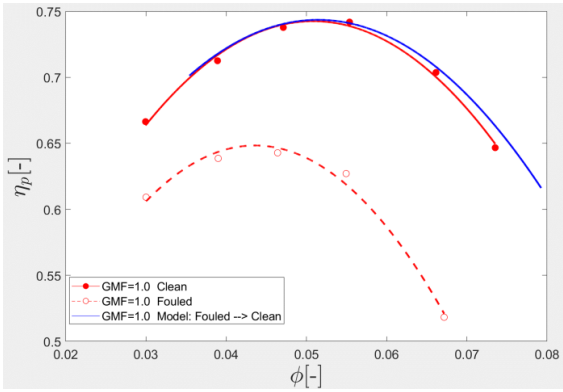

Figure 38 Correction from dry fouled to dry clean.

The resulting correction shows a reasonable fit between the clean curve and the fouled curve corrected to clean condition, although some deviations are seen in the high-flow region.

For the remaining curves, i.e., wet curves of varying *GMF* clean and fouled, a continuation of this approach was attempted. The idea was to incorporate a homogeneous gas-liquid mixture viscosity and the homogeneous density into

the calculation of the friction coefficient. The Dukler homogeneous viscosity model [12] was applied. This model is given by:

$$\mu_m = \rho_m \left[GMF \left(\frac{\mu_g}{\rho_g} \right) + (GMF - 1) \left(\frac{\mu_l}{\rho_l} \right) \right] \tag{63}$$

This homogeneous viscosity was used to calculate a new Reynolds number, based on homogeneous wet conditions, which was then used to calculate a new Darcy friction factor. The Reynolds number in wet condition was given by

$$Re_m = \frac{\rho_m u b}{\mu_m} \tag{64}$$

Where ρ_m is the homogeneous model gas-liquid mixture density given by Eq.(7). The friction factor based on the homogeneous viscosity was then used in Eq.(62). The same c as established for the dry curves was used. The resulting correction from all conditions to the clean dry condition is given in

Figure 39.

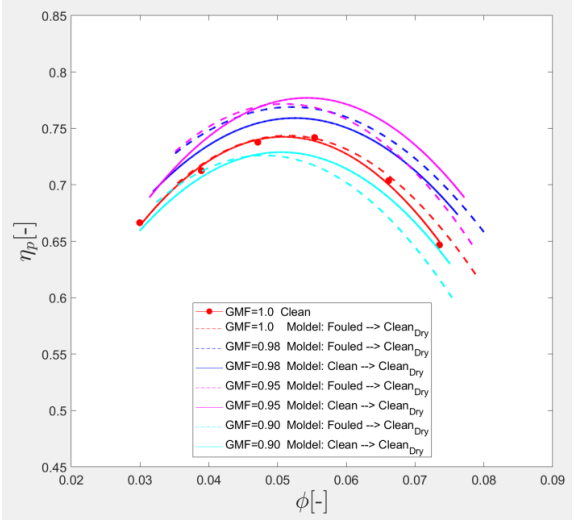

Figure 39 *GMF* adjusted ICAAMC similar method, utilizing homogeneous viscosity friction factor.

Overall, the proposed model does reduce the scatter in the efficiency curves. It manages to collect the curves for clean and fouled conditions (of the same *GMF*) to a large degree, but it does not seem to correctly account for the effect of different *GMF*s. However, by combining the model for the shift in performance between the clean and fouled conditions given here, together with the proposed model for wet gas performance given in section 5.2, it is suspected that the complete behaviour could be modeled.

5.4.2 Summary

In the scientific literature, little has been written about performance deterioration caused by fouling in wet gas centrifugal compressors. Therefore, this work represents a significant contribution to increased knowledge on the topic. The main test results can be summarized as:

- Wet performance characteristics are heavily affected by flow path fouling.
- The shift in wet characteristics relates to flow capacity, polytropic head and efficiency.
- All clean performance curves (for one speed) have similar shapes to each other, and all fouled curves (for one speed) have similar shapes to each other.
- The choke area of the wet performance characteristic is affected more than the surge area.

A first approach correction model for fouling in dry and wet conditions was developed. By applying the homogeneous mixture density and a model for wet viscosity into the machine Reynolds number, a model linking the increase in friction factor due to fouling to the efficiency drop was developed.

- The proposed model demonstrates the capability of correcting the shift in efficiency due to fouling in dry conditions. It also manages to collect the curves for clean and fouled conditions (of the same *GMF*) to a large degree, but it does not seem to correctly account for the effect of different *GMF*s.

6 CONCLUSION

The current work includes theoretical considerations, analysis of experimental results and development of models relating to the performance evaluation of wet gas centrifugal compressors. Several challenges relating to the performance evaluation of the wet gas compressor have been addressed. These relate to the design phase, performance testing and the operating phase.

- The wet gas compression process is associated with a highly complex flow field. The wet flow interacts with partly rotating and partly stationary parts. Furthermore, the flow is exposed to high velocities as well as very high accelerations and decelerations. In this thesis, it has been documented that theoretical similarity between different operating conditions in such complex flow fields is a challenging task and that a general solution probably cannot be found. Consequently, Type2 testing for wet gas compressors may be difficult to achieve.

- However, a detailed analysis of test results from a two-impeller compressor has shown that by applying a novel method for modelling wet gas performance, it was possible to collect data points obtained under different operating conditions onto a “performance surface” with good precision.

- It has been documented that the Monte Carlo Method is the recommended method for determining uncertainties in a complex system, such as a wet gas compressor test facility, which operates on hydrocarbons under real conditions. Furthermore, it has been demonstrated that somewhat greater uncertainties can be expected in wet performance parameters compared to dry, but still within acceptable limits. By including a torque meter and a gas density meter in the wet gas test facility, uncertainties of performance parameters can be reduced significantly.

- Fouling has been shown to have a detrimental effect on wet gas compressor performance. By building on the well-established ICAAMC procedure for Reynolds number correction, a fouling correction model was developed. The model linked the increase in friction factor due to fouling to the efficiency drop, where a homogeneous mixture density and wet viscosity was included in the machine Reynolds number. The model was capable of collecting the spread between clean and fouled efficiency curves for the same *GMF*.

The field of wet gas compression is relatively new, and a solid theoretical foundation is lacking. This thesis contributes to increased knowledge of wet gas compressor performance and will thus contribute to increasing overall knowledge in the field. The current work is a step toward developing test and evaluation standards that will help future projects. This work could be an enabler for the choice of wet gas compression in future projects, by helping operators predict performance change for shifting inlet conditions and by helping vendors design machines that will meet the design targets.

7 FURTHER WORK

There is still much to learn concerning the performance of wet gas centrifugal compressors. Based on experiences and findings that have emerged as part of this thesis, some recommendations for further work follow.

A recommendation for further work would be to rebundle the K-Lab compressor to include only one impeller and to run a wet gas test at both NTNU and K-Lab on a geometrically similar impeller to investigate whether performance data found at NTNU in water/air under ambient conditions could be transferred to real hydrocarbon gas/oil/water conditions at K-Lab. For such a test, the NTNU compressor should be modified from an axial inlet to a radial inlet compressor. In this way, it is possible to investigate whether test results obtained under ambient air/water conditions could be related to realistic conditions in a similar manner as Type2 testing is conducted in ASME PTC10. Furthermore, if there are limitations for when water/air can be compared to realistic conditions, these could be uncovered and documented.

Further investigation of the effect of varying viscosity is recommended to check if the method introduced in section 4.2 is still able to model the performance shifts between operating conditions. This could be done by expanding the temperature range of the test matrix, and another possibility could be to test using oils with significantly differing viscosity. Further analysis of methods to avoid overfitting when using the proposed method is also recommended.

It is recommended to perform an uncertainty analysis where the uncertainties of the characterization from plus to characterized fluid can be included. This investigation requires PVT software where the characterization can be performed programmatically. One example is the open-source software NeqSim. Further investigation of correlations arising from the normalization of compositional data is also recommended. There are at least two issues that should be investigated further. First, the appropriate method for estimating standard deviations of compositional data arising from the gas chromatography of both gas and oil samples should be established. Secondly, the appropriate method for randomly sampling compositional data for the MCM should be found.

The proposed fouling model demonstrated the capability of correcting the shift in efficiency between curves for clean and fouled conditions (of the same *GMF*) to a large degree, but it did not seem to correctly account for the effect of different *GMF*s. It is recommended to investigate if one could utilize a model of the type introduced in section 4.2 for the wet performance shift and combine this with the fouling model. In this way, one should be able to capture both the effect of fouling and the changing *GMF*.

REFERENCES

[1] Directorate, Norwegian Petroleum, 2021, "The Shelf 2021." https://www.npd.no/globalassets/1-npd/publikasjoner/sokkelaret/sokkelaret-2021/sokkelaret-2021-engelsk.pdf.

[2] "ASME PTC 10-1997, Performance test code on compressors and exhausters." American Society of Mechanical Engineers, New York.

[3] "ISO 5389 - Turbocompressors - Performance test code."

[4] Bøe, Caroline, Hjelmeland, Mads, and Torkildsen, Bernt Helge, "Gullfaks Subsea Compression: Early Operational Experience from the World's First Subsea Wet Gas Compression System." *Proc. Offshore Technology Conference*, OnePetro,

[5] Kleynhans, George, Brenne, Lars, Kibsgaard, Svend, and Dentu, Pascal, "Development and Qualification of a Subsea Compressor." *Proc. Offshore Technology Conference*, Offshore Technology Conference,

[6] Hedne, PE, Aarvik, A, Nordsveen, M, Pettersen, BH, and Hauge, LE, "Åsgard Subsea Compression-technology overview and operational experience." *Proc. 18th International Conference on Multiphase Production Technology*, OnePetro,

[7] Hjelmeland, Mads, and Torkildsen, Bernt Helge, "Qualification and Implementation of a Subsea Wet Gas Compressor Solution." *Proc. Offshore Technology Conference*, OnePetro,

[8] "MAN Energy Solutions." https://www.man-es.com/company/press-releases/press-details/2021/08/31/man-energy-solutions-to-deliver-subsea-compression-technology-for-jansz-io.

[9] Hundseid, Øyvind, Bakken, Lars E, Grüner, Trond G, Brenne, Lars, and Bjørge, Tor, "Wet Gas Performance of a Single Stage Centrifugal Compressor." *Proc. ASME Turbo Expo 2008: Power for Land, Sea, and Air*, American Society of Mechanical Engineers, pp. 661-670. DOI 10.1115/GT2008-51156

[10] Fabbrizzi, Michelangelo, Cerretelli, Ciro, Del Medico, Francesco, and D'Orazio, Maria, "An experimental investigation of a single stage wet gas centrifugal compressor." *Proc. ASME Turbo Expo 2009: Power for Land, Sea, and Air*, American Society of Mechanical Engineers, pp. 443-453

[11] Hall, A, Griffin, D, and Steven, R, "A discussion on wet gas flow parameter definitions." *Proc. 26th International North Sea Flow Meter Workshop, organized by the National Engineering Laboratory, East Kilbride, Scotland, UK*

[12] Awad, M. M., and Muzychka, Y. S., 2008, "Effective property models for homogeneous two-phase flows." *Experimental Thermal and Fluid Science*, 33(1), pp. 106-113. DOI 10.1016/j.expthermflusci.2008.07.006

[13] Lockhart, RW, and Martinelli, RC, 1949, "Proposed correlation of data for isothermal two-phase, two-component flow in pipes." *Chem. Eng. Prog*, 45(1), pp. 39-48

[14] Hundseid, Øyvind, and Bakken, Lars E, "Wet Gas Performance Analysis." *Proc. ASME Turbo Expo 2006: Power for Land, Sea, and Air*, American Society of Mechanical Engineers, pp. 625-632

[15] Wood, Albert Beaumont, 1949, A textbook of sound: being an account of the physics of vibrations with special reference to recent theoretical and technical development. G. Bell and sons, ltd.

[16] Kazi, Salim Newaz, 2012, "An overview of heat transfer phenomena."

[17] Schultz, John M., 1962, "The Polytropic Analysis of Centrifugal Compressors." *Journal of Engineering for Power*, 84(1), pp. 69-82. DOI 10.1115/1.3673381

[18] Zeuner, Gustav, 1907, "Technical Thermodynamics." (1st Engl. ed)

[19] Huntington, R. A., 1985, "Evaluation of Polytropic Calculation Methods for Turbomachinery Performance." *Journal of Engineering for Gas Turbines and Power*, 107(4), pp. 872-876. DOI 10.1115/1.3239827

[20] Wilsak, R. A., and Tatara, R. A., 2020, "Reassessing Polytropic Compressor Calculations of ASME PTC 10." *Energy Management Research Journal*, 3(1)

[21] Bertoneri, Matteo, Wilcox, Melissa, Toni, Lorenzo, and Beck, Griffin, "Development of test stand for measuring aerodynamic, erosion, and rotordynamic performance of a centrifugal compressor under wet gas conditions." *Proc. ASME Turbo Expo 2014: Turbine Technical Conference and Exposition*, American Society of Mechanical Engineers,

[22] Brenne, Lars, Bjørge, Tor, Gilarranz, José L, Koch, J, and Miller, Harry, "Performance Evaluation of a Centrifugal Compressor Operating under Wet-Gas Conditions." *Proc. Proceedings of the 34th Turbomachinery Symposium*, pp. 111-120. DOI 10.21423/R1V35Z

[23] Hundseid, Øyvind, and Bakken, Lars E., "Integrated Wet Gas Compressor Test Facility." *Proc. ASME Turbo Expo 2015: Turbine Technical Conference and Exposition*V009T24A011. DOI 10.1115/GT2015-43004

[24] 1980, "ASME PTC 19.23 Guidance Manual for Model Testing."

[25] Buckingham, Edgar, 1914, "On physically similar systems; illustrations of the use of dimensional equations." *Physical Review*, 4(4), p. 345

[26] Nguyen, DL, Winter, ERF, and Greiner, M, 1981, "Sonic velocity in two-phase systems." *International Journal of Multiphase Flow*, 7(3), pp. 311-320

[27] Kieffer, Susan Werner, 1977, "Sound speed in liquid‐gas mixtures: Water‐air and water‐steam." *Journal of Geophysical research*, 82(20), pp. 2895-2904

[28] Beattie, DRH, and Whalley, PB, 1982, "A simple two-phase frictional pressure drop calculation method." *International Journal of Multiphase Flow*, 8(1), pp. 83-87

[29] Rutgers, Ir R, 1962, "Relative viscosity and concentration." *Rheologica Acta*, 2(4), pp. 305-348

[30] ISO, IEC, OIML, and BIPM, 1995, "Guide to the Expression of Uncertainty in Measurement." *Geneva, Switzerland*, 122

[31] Test Uncertainty, ASME, 2018, "PTC 19.1-2018." American Society of Mechanical Engineers, pp. 10016-15990.

[32] ISO, ISO, 2008, "98-3/Suppl. 1: Uncertainty of Measurement—Part3: Guide to the Expression of Uncertainty in Measurement (GUM: 1995) Supplement 1: Propagation of Distributions Using a Monte Carlo Method." *ISO: Geneva, Switzerland*

[33] Mæland, Dagfinn, 2020, July 17, "Source Code." https://doi.org/10.5281/zenodo.3988097.

[34] Aitchison, John, 1981, "A new approach to null correlations of proportions." *Journal of the International Association for Mathematical Geology*, 13(2), pp. 175-189

[35] "ISO 6974-3:2018 Natural gas - Determination of composition and associated uncertainty by gas chromatography - Part 3: Precision and bias."

[36] Pawlowsky-Glahn, Vera, Egozcue, Juan José, and Tolosana-Delgado, Raimon, 2015, Modeling and analysis of compositional data. John Wiley & Sons.

[37] Saltelli, Andrea, Aleksankina, Ksenia, Becker, William, Fennell, Pamela, Ferretti, Federico, Holst, Niels, Li, Sushan, and Wu, Qiongli, 2019, "Why so many published sensitivity analyses are false: A systematic review of sensitivity analysis practices." *Environmental modelling & software*, 114, pp. 29-39

[38] Saltelli, Andrea, Ratto, Marco, Andres, Terry, Campolongo, Francesca, Cariboni, Jessica, Gatelli, Debora, Saisana, Michaela, and Tarantola, Stefano, 2008, Global sensitivity analysis: the primer. John Wiley & Sons.

[39] Simon, H., and Bülskämper, A., 1984, "On the evaluation of Reynolds number and relative surface roughness effects on centrifugal compressor performance based on systematic experimental investigations." *Journal of Engineering for Gas Turbines and Power*, 106(2), pp. 489-498. DOI 10.1115/1.3239592

[40] Strub, R. A., Bonciani, L., Borer, C. J., Casey, M. V., Cole, S. L., Cook, B. B., Kotzur, J., Simon, H., and Strite, M. A., 1987, "Influence of the Reynolds Number on the Performance of Centrifugal Compressors." *Journal of Turbomachinery*, 109(4), pp. 541-544. DOI 10.1115/1.3262145

[41] Colebrook, C. F., Blench, T., Chatley, H., Essex, E. H., Finniecome, J. R., Lacey, G., Williamson, J., and Macdonald, G. G., 1939, "Correspondence. Turbulent Flow in Pipes, with Particular Reference to the Transition Region between the Smooth and Rough Pipe Laws. (Includes Plates)." *Journal of the Institution of Civil Engineers*, 12(8), pp. 393-422. DOI 10.1680/ijoti.1939.14509

[42] Nikuradse, Johann, 1950, "Laws of flow in rough pipes." No. NACA TM 1292, National Advisory Committee for Aeronautics Washington

[43] Casey, M. V., 1985, "The Effects of Reynolds Number on the Efficiency of Centrifugal Compressor Stages." *Journal of Engineering for Gas Turbines and Power*, 107(2), pp. 541-548. DOI 10.1115/1.3239767

[44] Kunz, Oliver, and Wagner, Wolfgang, 2012, "The GERG-2008 wide-range equation of state for natural gases and other mixtures: an expansion of GERG-2004." *Journal of chemical & engineering data*, 57(11), pp. 3032-3091

[45] Glen, NF, Mills, D, Griffin, Douglas, and Fosse, S, "Errors Due to Use of the AGA8 Equation of State Outside of Its Range of Validity." *Proc. Offshore Technology Conference Asia*, Offshore Technology Conference,

[46] Van der Waals, Johannes Diderik, 1873, Over de Continuiteit van den Gas-en Vloeistoftoestand. Sijthoff.

[47] Redlich, Otto, and Kwong, Joseph NS, 1949, "On the thermodynamics of solutions. V. An equation of state. Fugacities of gaseous solutions." *Chemical reviews*, 44(1), pp. 233-244

[48] Soave, Giorgio, 1972, "Equilibrium constants from a modified Redlich-Kwong equation of state." *Chemical engineering science*, 27(6), pp. 1197-1203

[49] Peng, Ding-Yu, and Robinson, Donald B, 1976, "A new two-constant equation of state." *Industrial & Engineering Chemistry Fundamentals*, 15(1), pp. 59-64

[50] Solbraa, Even, 2002, "Equilibrium and non-equilibrium thermodynamics of natural gas processing."

[51] Michelsen, Michael L, 1982, "The isothermal flash problem. Part I. Stability." *Fluid phase equilibria*, 9(1), pp. 1-19

[52] Michelsen, Michael L, 1982, "The isothermal flash problem. Part II. Phase-split calculation." *Fluid phase equilibria*, 9(1), pp. 21-40

[53] Rachford Jr, HH, and Rice, JD, 1952, "Procedure for use of electronic digital computers in calculating flash vaporization hydrocarbon equilibrium." *Journal of Petroleum Technology*, 4(10), pp. 19-13

PAPER I

PAPER II

PAPER III

PAPER IV

This paper is not included due to ASME copyright

APPENDIX A - EQUATIONS OF STATE, MIXING RULES AND FLASH CALCULATIONS

The theoretical basis for equations of state: Real gas equations of state are extensions of the ideal gas law $PV_m = RT$. In 1873, van der Waals proposed his famous equation of state which accounts for the volume occupied by the molecules as well as intermolecular forces [46]:

$$P = \frac{RT}{V_m - b} - \frac{a}{V_m^2} \tag{65}$$

Here the constants a and b are called the van der Waals Coefficients, where a is a constant for the attractive forces between molecules and b is associated with the volume occupied by the molecules. These coefficients are estimated from the critical properties of the fluid, T_c and P_c. In 1948 the Redlich-Kwong equation of state was published [47]. This equation was further developed and in 1972 Soave presented the Soave-Redlich-Kwong (SRK) equation of state [48], which gives better results for vapour pressure both for pure substances and for mixtures, this equation is given as:

$$P = \frac{RT}{V_m - b} - \frac{a(T)}{V_m(V_m + b)} \tag{66}$$

Using the real gas equation, $PV_m = ZRT$, and letting

$$\frac{aP}{R^2T^2} = A \tag{67}$$

and

$$\frac{bP}{RT} = B \tag{68}$$

it can be shown that the SRK equation can be written as:

$$Z^3 - Z^2 + Z(A - B - B^2) - AB = 0 \tag{69}$$

Thus, the SRK is called a cubic EOS.

The coefficients for, a, and b are calculated as:

$$b = \frac{0.08664RT_c}{P_c} \tag{70}$$

$$a(T) = a_c\alpha(T) \tag{71}$$

Where

$$a_c = \frac{0.42747 R^2 T_c^2}{P_c} \tag{72}$$

$$\alpha(T) = \left(1 + m\left(1 - \sqrt{\frac{T}{T_c}}\right)\right)^2 \tag{73}$$

$$m = 0.480 + 1.574\omega - 0.176\omega^2 \tag{74}$$

Here the acentric factor ω is an empirical constant that is associated with the molecular deviation in shape from that of a sphere and is established by $\omega = -1 - \log_{10}\left(\frac{P^{sat}}{P_c}\right)_{T=0.7T_c}$.

As the SRK has some shortcomings when it comes to predicting liquid densities and the Peng-Robinson (PR) equation was developed presented in 1976 [49], the PR equation is given as:

$$P = \frac{RT}{V_m - b} - \frac{a(T)}{V_m(V_m + b) + b(V_m - b)} \tag{75}$$

Similarly, as for SRK, it can be shown that the PR equation is also a cubic EOS.

Mixing Rules: For the EOS to be useful not only for pure components, it also needs to be able to handle phase equilibrium for mixtures. To allow for the use of the EOS for mixtures, mixing rules need to be introduced to describe how the EOS parameters can be expressed for these mixtures. One common mixing rule called the van der Waals mixing rule [50] is given as:

$$a = \sum_i \sum_j z_i z_j a_{ij} \tag{76}$$

$$b = \sum_i \sum_j z_i z_j b_{ij} \tag{77}$$

Where

$$a_{ij} = \sqrt{a_i a_j}(1 - k_{ij}) \tag{78}$$

$$b_{ij} = \frac{b_i + b_j}{2} \tag{79}$$

Where k_{ij} are the empirically determined binary interaction coefficients. For two nonpolar components, k_{ij} is close to 0 for two polar components, k_{ij} is close to 0, and for two components where one is polar, and one is nonpolar the k_{ij} is different from 0. One example is k_{ij} for water-hydrocarbon, is typically 0.5. It is important to note that the only addition to the pure component parameters, T_c, P_c, ω, is the binary interaction coefficients k_{ij}. With the availability of these binary interaction parameters and a mixing rule, the EOS can be used for mixtures.

The theoretical basis for the flash calculation: The isothermal flash is the flash of a composition taken at a specific pressure and temperature. This is the most widely used flash.

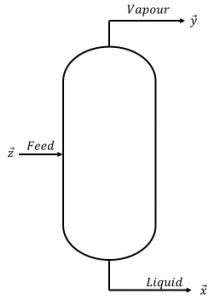

Figure 40 Basic two-phase Flash

The isothermal (P/T) flash problem has a unique solution that corresponds to the global minimum of the Gibbs energy of the mixture. Although a unique solution is guaranteed, the number of equilibrium phases in the solution is not known in advance and algorithms such as stability analysis for determining the number of equilibrium phases must be built into the models [51, 52].

In a hydrocarbon vapour-liquid equilibrium flash where the stability test indicates two phases, the equilibrium constant is given by:

$$K_i = \frac{y_i}{x_i} = \frac{\varphi_i^l}{\varphi_i^v} \tag{80}$$

Where y_i and x_i are the mole fraction of the i-th component of the vapour and liquid phase, respectively. By utilizing this expression together with the material balance $V + L = 1$, where V and L is vapour phase fraction (molar basis) and liquid phase fraction (molar basis), respectively one gets

$$y_i = \frac{K_i z_i}{(K_i - 1)V + 1} \tag{81}$$

$$x_i = \frac{z_i}{(K_i - 1)V + 1} \tag{82}$$

and further utilizing the fact that $\Sigma(y_i - x_i) = 0$ one arrives at the Rachford-Rice equation [53]

$$F(V, K_1, K_2, \dots, K_n, z_1, z_2, \dots, z_n) = \sum_i \frac{(K_i - 1)z_i}{(K_i - 1)V + 1} = 0 \tag{83}$$

For a given set of K_i values and feed composition values z_i, Eq.(83) can be solved for V. One procedure for solving the flash problem is then:

1. Guess an initial set of Ki
2. Find the V by solving Eq.(83)
3. Find the gas and liquid compositions from Eq.(81) and Eq.(82), respectively.
4. Find the fugacity coefficients φ_i^v and φ_i^l by a selected equation of state
5. Update $K_i = \frac{\varphi_i^l}{\varphi_i^v}$
6. Repeat from 2 until K_i converge

This method of direct substitution generally converges, and a method for accelerating convergence is given by Michelsen [52]. For three-phase flash calculations including gas, oil, and water phase reference is given to the work by Michelsen [52].